Characterization of Several Small Biologically Relevant Molecules by Infrared Multiple Photon Dissociation Spectroscopy and Electronic Structure Calculations

by

Sabrina M. Martens

A thesis
presented to the University of Waterloo
in fulfillment of the
thesis requirement for the degree of
Master of Science
in
Chemistry

Waterloo, Ontario, Canada, 2011

AUTHOR'S DECLARATION

I hereby declare that I am the sole author of this thesis. This is a true copy of the thesis, including any required final revisions, as accepted by my examiners.

I understand that my thesis may be made electronically available to the public.

Abstract

Infrared multiple photon dissociation (IRMPD) spectroscopy has been coupled with electronic structure calculations in order to elucidate the structures of several small biological molecules including: uracil, 5-fluorouracil, 5-fluorocytosine, ferulic acid, and a number of their related analogs. IRMPD is a powerful technique, that when combined with electronic structure calculations can provide convincing evidence for the structural characterization of ions in the gas phase.

Isomers of uracil and 5-fluorouracil (5-FU) have been characterized by calculations performed at the MP2(full)/aug-cc-pVTZ level of theory; however, infrared multiple photon dissociation spectroscopy experiments proved to be unsuccessful for these species. Geometry optimization and frequency calculations have isolated the dominant isomer(s) for neutral and deprotonated uracil and 5-fluorouracil, along with several cluster interactions involving water, methanol, ammonia, and methylamine. For both uracil and 5-FU, a single relevant neutral isomer was determined, with each isomer existing in the diketo, as opposed to the enol form. Following the deprotonation of this neutral isomer, both uracil and 5-FU were permitted to form anionic cluster ions with water, methanol, ammonia, or methylamine, and based on the relative Gibbs free energies (298 K) of the calculated isomers, relevant cluster interactions were determined. For each cluster, several sites of intramolecular interaction were found to exist; however, interaction at the site of deprotonation was the most favourable in every instance.

Ionic hydrogen bond interactions have been found in several clusters formed by 5-fluorocytosine (5-FC). The chloride and trimethylammonium cluster ions, in addition to the cationic and anionic dimers have been characterized by infrared multiple photon dissociation (IRMPD) spectroscopy and electronic structure calculations performed at the B2PLYP/aug-cc-pVTZ//B3LYP/6-311+G(d,p) level of theory. IRMPD spectra in combination with calculated spectra and relative energetics have indicated, quite conclusively, that a single isomer for each 5-FC cluster that is likely being observed experimentally except in the case of the anionic dimer, in which a combination of isomers is probable. For the 5-FC-trimethylammonium cluster specifically, the calculated spectrum of the lowest energy isomer matches the experimental spectrum remarkably well. Interestingly, the cationic dimer of 5-FC was found to have a single energetically relevant isomer (Cationic-IV) in which a unique tridentate ionic hydrogen bond interaction is formed. The three sites of intramolecular ionic hydrogen bonds in this isomer interact very efficiently, leading to a significantly large calculated enthalpy of binding of 180 kJ/mol. The magnitude of the calculated binding energy for this species, in combination with the strong correlation between the simulated and IRMPD spectra, indicates that the tridentate-bound dimer is observed predominantly in experiment. Comparison of the calculated relative Gibbs free energies (298 K) for this species with several of the other isomers considered also supports the likelihood of the dominant protonated dimer existing as Cationic-IV.

Protonated ferulic acid has been characterized using infrared multiple photon dissociation spectroscopy and electronic structure calculations at the B3LYP/6-311+G(d,p) level of theory. Neutral ferulic acid has been determined to undergo protonation on the

carbonyl oxygen of the acid group, forming an ion of m/z 195. Due to its extensively conjugated structure, protonated ferulic acid (m/z 195) is observed to yield three stable fragment ions in IRMPD experiments. It is proposed that two parallel fragmentation pathways of protonated ferulic acid are being observed. First, proton transfer occurs from the carbonyl oxygen to the hydroxyl oxygen within the acid group, resulting in the loss of water and subsequently carbon monoxide, forming ions of m/z 177 and 149, respectively. The second proposed fragmentation pathway undergoes proton transfer from the phenolic group to the methoxy group resulting in loss of methanol and rearrangement to a five-membered ring of m/z 163. IRMPD spectra have been obtained for the ions m/z 195 and m/z 177, and anharmonic calculations have been performed on these species at the B3LYP/6-311+G(d,p) level of theory. The calculated anharmonic spectra for these ions match the experimental spectrum exceptionally well and strongly support the proposed fragmentation mechanisms.

Acknowledgements

I would like to thank my supervisor, Terry McMahon. Terry has always treated me with great respect and provides his students with freedom. I have been able to become truly passionate about chemistry because he facilitates the freedom to be creative and inspires his students to be motivated and productive. Terry's excitement about chemistry is truly contagious and his passion makes what some may find "uninteresting" look fantastic. I have been given the opportunity to conduct research in France twice and present in several conferences, which I am very thankful for. Because of Terry, I am able to say that graduate school has been a wonderful experience in which I have learned a tremendous amount.

I would like to thank the members of my committee, Bill Power and Pierre-Nicholas Roy for agreeing to be on my committee and for taking the time to read my thesis.

I would like to acknowledge my mother, Marie Martens, for many reasons. Mom, you are a highly intelligent person who has taught me that I can do whatever I want, if I am willing to put in the effort. As long as I can remember, you have been teaching me, and I must attribute my grammar and writing skills to you! You are an amazing piano player and I will always have pleasant memories of you playing your piano in the background as I studied. It is inspiring to see you succeed at everything you do. I love our days we spend together just grabbing a coffee and going to the mall. In you, I have both a best friend and a mother. Most of all, I must thank you for your unconditional love. You are the most loving person I know and you have poured your heart into raising us. Your never ending support has made me believe in myself, that I can accomplish anything I put my mind to.

I would also like to acknowledge my father, Ken Martens, for everything he has done for me. Dad, you are the most multi-faceted person I have ever met! I have no doubt that there is nothing you cannot do. It is amazing to watch you work on the house doing every job, jobs which people take a lifetime to perfect, like a pro. You are an excellent father and I have always loved the time we spend together, whether it is fishing, last minute Christmas shopping, or just grabbing a coffee. You have taught me to take pride in everything I do, no matter how small, and to always do my best.

I would also like to thank Rick Marta who has taught me so much. Rick, you always make yourself available to help me, no matter how busy you are and you have taught me to be excited about chemistry. You are an exceptional teacher and I am not at all surprised at your continued success. You have made working in the lab a fun, enjoyable, and productive experience. I cannot express my gratitude for all of my writing you have edited, concepts you have explained, and the overall support you have shown. Even when I get overwhelmed or doubt myself, you are always there to convince me I will be alright, encourage me, and help me succeed. Your help has made all the difference to me, thank you so much, I love you!

I would like to thank my brother, Jon Martens, who is the reason why I joined the McMahon lab in the first place. Jon, you have never treated me like an "annoying little sister", but always like a friend. I cannot even count how many hours we played Mario Kart 64 together after long days in the office. I really appreciate that you let me come around and study in your office when you were just starting out your PhD. Your passion for chemistry is really what made me discover that I also had a passion for chemistry!

My dog Scooter must be acknowledged for his never ending devotion and loyalty. You were my four pound "live-teddy bear" and we have been inseparable for the past nine years. I can't express how much you meant to me and I will miss you every day for the rest of my life. No matter how long the days and nights of studying or writing may have been, you never left my side. Your constant presence made me never feel alone. You were the perfect dog and I am blessed to have ever had you, even if you were taken from me too early. I love you.

I would like to acknowledge Paula Kuipery who has been my best friend since the moment I met her in grade 12. Paula because of you, I feel like I have experienced a big part of life that I otherwise would have missed out on. We are both very busy and have helped keep each other sane throughout it all. Beginning with undergrad, there would be times where we would be so exhausted from studying, but we would always talk, laugh, and make plans to look forward to. I don't know what I would do without a friend like you!

I would like to acknowledge my grandmother Odette Favis and my late grandfather Dimitrios Favis. Grandmaman it has been a great support to know that you are praying for me when I am nervous about a big exam, interview, etc. You always make a note of important events in my life and always remember to ask me how they went. Grandpapa, I know you would have taken great pride in me joining the field of chemistry in your footsteps. I would have loved to be able to talk about chemistry with you, and have you read my thesis. You were an exceptionally intelligent man with such great accomplishments. It makes me very proud to know that chemistry runs in the family!

I would also like to thank my grandparents John and Kay Martens. Thank you for your continued support.

I would also like to acknowledge my uncle, Basil Favis. You are always fun to be around and have always encouraged me in the area of chemistry. It makes me proud to have another member of my family, who has been so successful in the field of chemistry, whose footsteps I can follow in.

I would like to thank Lynn Rivait who works at the EIT coffee shop. Lynn always has a smile on her face and something funny to contribute, often making my coffee breaks the highlight of long workdays.

Finally, I would like to thank Cathy Van Esch, the administrative coordinator for graduate studies in chemistry. Cathy has been very patient and has always gone out of her way to assist me, regardless of whether it was in her "job description".

Dedication

I dedicate my thesis to my parents:

Ken and Marie Martens

for their never ending support

AND

In memory of:

my beloved Scooter,

a true friend and the best dog ever.

2002-2011

Table of Contents

List of Figures

List of Tables

Chapter 1
Introduction

1.1 Ionic Hydrogen Bonding in the Gas Phase

Hydrogen bonds are considered to be one of the most important intermolecular forces and as such, have been a popular subject of research for almost a century.[1-4] Hydrogen bonds typically involve a linear association between a donor "A-H" and an acceptor "B" linked by the hydrogen atom, where A and B are both electronegative elements.[5-6] The bond strengths of hydrogen bonds can range from weak to very strong. When a hydrogen bond containing a proton is formed during an ion-molecule association reaction, it is referred to as an ionic hydrogen bond or IHB.[7] IHBs typically have bond strengths in the range of 20-150 kJ/mol.[1, 4, 8] Strong hydrogen bonding typically occurs when the proton is equally attracted to both A and B, but not evidently covalently bonded to either.[5] Strong hydrogen bonds are considered to be different enough from "normal" hydrogen bonds that they are sometimes considered to consist as a separate category of interactions.[5] In fact, the upper range of the bond strengths of IHBs is in some cases greater than the strength of some covalent bonds, such as F_2, which has a bond energy of 155 kJ/mol.[9] IHBs are very important interactions which are critical in many chemical processes such as ionic clusters, electrolytes, nucleation, acid-base chemistry, ionic crystals, and surface adsorption.[1] Over the past forty years, there have been a plethora of studies related to IHB formation.[1, 10-14] Research related to hydrogen bonds is still a important field of study because they play a major role in many chemical and biochemical pathways and the fundamentals of their properties need to be understood.

Ionic hydrogen bonds are capable of forming in both cationic and anionic systems.[1] A representation of a system involving a cationic IHB formation in the gas phase is shown below in equation 1.1.

$$M + MH^+ \rightarrow [M\cdots H\cdots M]^+ \qquad \textbf{[1.1]}$$

In equation 1.1, M is a neutral monomer species containing at least one Lewis basic heteroatom and MH^+ is the protonated monomer. The product formed in equation 1.1 is a symmetric proton-bound dimer (PBD). The formation of this IHB involves partial proton transfer from the hydrogen donor atom to the acceptor, and the bond strength is correlated with the efficiency of proton transfer. The original bond length between the hydrogen and donor heteroatom increases in length and the charge is shared with the acceptor. As a result, the acceptor and donor atoms become more negative and the proton involved in the IHB becomes more positive.[1] If the formation of an IHB results in a heterodimer, the bond will be the strongest when the proton affinities of the donor and acceptor are similar. If the IHB results in a homodimer however, the proton affinities of the components will be identical, and the strength of the ionic hydrogen bond will not be affected by the value of the proton affinities.[1]

Many biological species and complex biological systems rely on the formation of ionic hydrogen bonds including: protein folding, enzymes, proton transport, and molecular recognition.[1] Biological molecules such as DNA and RNA nucleobases rely on hydrogen bonds for their three-dimensional structure and biological functionality.[15-17] Hydrogen bonds

also play a dominant role in the secondary and tertiary structure of proteins and largely effect their folding affinity.[6, 18] In fact, α-helices and β-sheets were first predicted in 1951 by Linus Pauling on the basis of hydrogen bonding.[19] Though these are just a few examples of hydrogen bonds in biological systems, they are decidedly important ones. When studying ionic hydrogen bonding interactions, it is thus sensible to research biologically relevant species, if possible.

Solvation is one of the most significant factors influencing the strength of hydrogen bonds and can be as (or more) important than the intrinsic molecular parameters themselves.[1, 8] Solvent effects are dramatic in their influence on hydrogen bond strength because prior to the formation of the hydrogen bond, the donor and acceptor are solvated.[8] Often the solvents present are also capable of forming hydrogen bonds and become competition for the formation of the non- solvent hydrogen bonds. The ability to form hydrogen bonds under solvent conditions is correlated to the properties of the solvent present, and in general, as the polarity of the solvent increases, the strength of the intramolecular hydrogen bond decreases.[8] Because of the dramatic effects solvent can have on hydrogen bonding interactions, and the differences observed based on which solvent is present, it becomes clear that studying these interactions in the gas phase is very useful, since the energetic and structural consequences associated with IHB formation can be intrinsically quantified.[7]

1.2 Mass-Selected Infrared Multiple Photon Dissociation (IRMPD) Spectroscopy

Infrared multiple photon dissociation (IRMPD) spectroscopy has been used in order to obtain gas-phase vibrational spectra. Ions are provided from a solution containing solvent and analyte using electrospray, a soft ionization technique. The desired ionic species can be isolated in the gas phase and confined within the quadrupole ion-trap mass spectrometer.[20] Trapped ions are irradiated and IRMPD follows by focusing a laser through a small opening in one of the ring electrodes to the center of the ion trap. The IRMPD process involves the use of a free electron laser (FEL) which is a powerful, tunable infrared light source that can be used to dissociate species isolated in the mass spectrometer. As different frequencies are scanned, vibrational modes can absorb energy at specific frequencies, resulting in fragmentation, given that IRMPD occurs. It has been established that in most cases the dissociation pathways are the same, no matter which mode in the molecule is excited.[21] This can be attributed to a process called intramolecular vibrational energy redistribution (IVR). The components of the experimental setup will be discussed in detail in Chapter 2.

1.2.1 The IRMPD Process

The process of infrared multiple photon dissociation has a very complex mechanism involving the unimolecular dissociation of ions due to the absorption of photons.[22] As will be discussed subsequently, the vibrations of molecules are often calculated using the harmonic oscillator approximation, a simplification in which the vibrational modes are considered independent of each other, but in reality the vibrational modes are typically

coupled together.[7] The process of IRMPD relies on the coupling of vibrational modes and by the process of intramolecular vibrational redistribution (IVR), energy can be randomized through the vibrations of the molecule. Upon the absorption of a photon, excitation of a single oscillator occurs, dependent on the number and wavelength of the absorbed photon.[23] If this single oscillator however, is coupled to the other vibrational modes in the molecule, the energy will flow to other oscillators which were not directly excited.[22] The energy can therefore be completely delocalized throughout the modes which are coupled. The process of IVR is considered to be faster than the time scale of molecular vibrations and therefore the energy is capable of being redistributed immediately.[7, 24] A molecule can rapidly have its total vibrational energy increased upon the sequential absorption of multiple photons, in which case the process of IVR allows dissociation throughout the coupled modes in the species.[22] If sufficient modes are coupled, the energy will reach the dissociation threshold of the weakest bond within the species and fragmentation will occur at that site.[7] However, if the vibrational mode which absorbs energy does not have an efficient IVR process, most likely due to an inability to redistribute energy to the weakest bond, then fragmentation is unlikely to occur.

During IRMPD experiments, it is not the direct absorption of photon energy that is measured, but the fragmentation efficiency due to the absorption of photons.[25] Because of this, the spectra obtained from these experiments are called consequence spectra and are considered an indirect measure of a species' photon absorption as a function of photon energy.[7] The IRMPD efficiency is therefore described by a relationship between the intensity of the parent ion and the fragments, and is expressed as:

$$IRMPD\ efficiency = -\log\left(\frac{I_{PARENT}}{I_{PARENT} + \sum I_{FRAGMENTS}}\right) \quad \textbf{[1.2]}$$

where I_{PARENT} and $I_{FRAGMENTS}$ represent the intensities of the parent ion and each of the fragment species, respectively. It is important to note that the relative intensities between the calculated and experimental spectra will vary. Since unimolecular dissociation of the parent ion relies upon having sufficient energy in the mode corresponding to the reaction coordinate, the intensity of the experimental spectrum will be dependent upon the IVR efficiency of the species, but also upon the laser power which can be subject to some fluctuations. The calculated vibrational spectrum is based upon the absorption intensities of vibrational modes for the species and does not account for the IVR process, or for fluctuations in laser power.

1.2.2 Applications and Relevance of IRMPD

IRMPD has become a very popular technique for the study of ions in the gas phase and is well suited for the study of ionic hydrogen bonds because they are ideally studied in an environment that effectively eliminates solvent effects. Traditional infrared spectroscopy is a fundamental technique for the study of the structures of molecules, but ions prove difficult to study because they are typically available in small number densities. [16, 26-27] Infrared multiple photon dissociation spectroscopy makes use of the sensitivity of a mass spectrometer in order to trap and detect ions in the gas phase. Recently, there have been a plethora of studies involving mass spectrometry and laser-induced photoactivation in order to study isolated ions in the gas phase.[7, 12-13, 21, 27-38]

Some of the earliest experiments, however, were performed several decades ago on weakly bound molecular clusters. Weakly bound clusters (approximately <20kJ/mol) are often capable of having dissociation induced by the absorption of a single photon and therefore, relatively low power laser sources could be used.[25] In the early 1980's, protonated hydrogen and protonated water clusters were studied by Lee and coworkers[39]. Later in the 1980's, more strongly bound species were able to be studied, such as several negatively charged complexes characterized by Beauchamp and coworkers using an FT-ICR mass spectrometer.[25, 40] In 1986, Zakin and coworkers performed the first observed IRMPD experiments on metal cluster-adsorbate complexes. IRMPD was used to determine the weakest bonds in the complex and also in order to obtain detailed information regarding the structures of the adsorbate, cluster and the adsorbate-cluster interactions. A test species involving methanol and iron was used, and the structural characterization was successful, demonstrating the feasibility of using IRMPD in order to study this type of complex.[41] In the 1990's, covalently bound molecules were studied by IRMPD using a free electron laser, and in 2000 the first IRMPD spectrum of an ionic species was published, due to the use of a free electron laser. Since then, many chemically interesting species have been studied and trapping techniques have been further developed. It is now possible for proton bound dimers, amino acids clustered with metal ions, and even an entire protein of 104 amino acid residues to be characterized using IRMPD.[13, 29, 42-43] In 2006, Polfer and coworkers studied tryptophan complexes involving several different metal ions in order to better characterize their binding.[43] IRMPD was found to characterize the metal-ligand binding superior to other mass spectrometry-based techniques.[43] The purpose of the study was to determine if the

zwitterion was present to any significant extent and also to determine the predominant structure, which were both able to be answered with fairly good certainty, using IRMPD experiments.[43] Today, IRMPD continues to be a popular method employed by physical chemists in order to characterize ions in the gas phase.

Chapter 2
Experimental Methods

2.1 Infrared Multiple Photon Dissociation Spectroscopy

The experimental component of the research presented in this thesis involves infrared multiple photon dissociation spectroscopy. IRMPD is a powerful and sensitive technique which has been proven to be very valuable in structure elucidation studies.[12, 38, 44-48] The components of the experimental setup are discussed in detail in the following sections.

2.1.1 Electrospray Ionization Interface

The concept of electrospray ionization was proposed by Dole in 1968 as a potential mechanism for the formation of ions from large molecules. However, it was not until 1984, that authentic experimental results were obtained for macromolecules and proteins of masses up to 40,000 Da.[49] Yamashita, Fenn, and Aleksandrov seemingly simultaneously produced and published these results.[49-50]

In original experiments involving electrospray mass spectrometry (ES-MS), a sample solution is prepared which contains the analyte, the desired solvent, and in some cases, the addition of a small amount of acid or base to aid in the formation of ions. This sample solution is then introduced into the electrospray chamber through a hypodermic needle at ground potential using a flow rate of around 1-40 μL/min.[51] Though the needle is not charged, the field surrounding the needle tip charges the surface of the liquid being sprayed

and scatters it into subsequently smaller, charged droplets. These droplets are drawn to the entrance of the capillary due to the electric field present and enter an environment with an increased temperature (~350 K).[51] As the ions enter the capillary they come in contact with a countercurrent flow of bath gas (generally N_2) which serves to sweep away any neutral species in addition to the evaporating solvent vapour. It has been suggested that as evaporation occurs, the charge to surface area ratio is no longer in balance due to the extremely small radius of curvature relative to the electric field at the droplet surface and Coulomb explosions can occur causing the analyte ions to desorb into the surrounding gas.[51] The desorbed ions then exit the capillary and pass through a skimmer into a vacuum chamber, allowing the ions to arrive at the mass spectrometer.

More recently however, the design of the electrospray source has become more advanced and its ionization mechanism better understood. Due to lower flow rates (0.1-10 μL/min), the analyte solution is simply pumped through a fine electrospray capillary (inner diameter ~100 μm) rather than a hypodermic needle.[49, 52] The capillary itself is charged with a voltage of between 2-5 kV and the emerging liquid forms a protrusion known as a Taylor cone, and at a certain threshold voltage, ejects a jet of liquid and a plume in which the ions can transfer to the gas phase.[49] Typically the initial droplets formed will have a diameter of more than 1 μm, and will therefore contain more than 150,000 analyte molecules per droplet.[49] In order to determine how analyte molecules are transferred to the gas phase, there has been continued extensive research on electrospray ionization. There are two widely proposed gas phase ion formation mechanisms, the charge-residue and ion-evaporation models. It has been suggested that both may have an application in describing the gas-phase

ionization process, based on the size of the ions. Although not definitively concluded, studies have suggested that for small ions (droplet on the order of 10^{-6} cm), the ion evaporation-model applies and for larger ions, the charge-residue model is more applicable.[53] The pairing of electrospray ionization with mass spectrometry in the 1980's and the rapid development and improvement of the instrumentation have allowed for a means to analyze many samples that are difficult to vapourize, such as nonvolatile, polar, and thermally labile species.[54]

2.1.2 Quadrupole Ion Trap

The quadrupole ion trap mass spectrometer is an important tool for the qualitative and quantitative analysis of ions. A quadrupole ion trap is made up of three uniquely shaped electrodes with hyperboloidal geometry. Two of these electrodes are end-cap electrodes, while the third, which is situated between the two end-cap electrodes, is shaped like a ring, and appropriately called the ring electrode.[55-56] The two end-cap electrodes are shaped like small inverted saucers and are virtually identical except for the number of small apertures found on each. The first has a single aperture allowing electrons or ions to be gated periodically. The second end-cap electrode may have one or several small apertures depending on whether there exists an external ion source, or the ions pass through to a detector, respectively.[55] The ring electrode is found symmetrically between the two end-cap electrodes, and can have an r.f. potential applied to it, while the two end-cap electrodes are grounded, thus creating a potential well from the field which exists.[55, 57] The geometries of the electrodes theoretically result in an ideal quadrupole field which produces the parabolic

potential well for the trapping of ions, based on the assumption that the electrodes go to infinity, producing asymptotes at 53° 34'.[55] The end-cap and ring electrodes are shown in Figure 2.1 below.

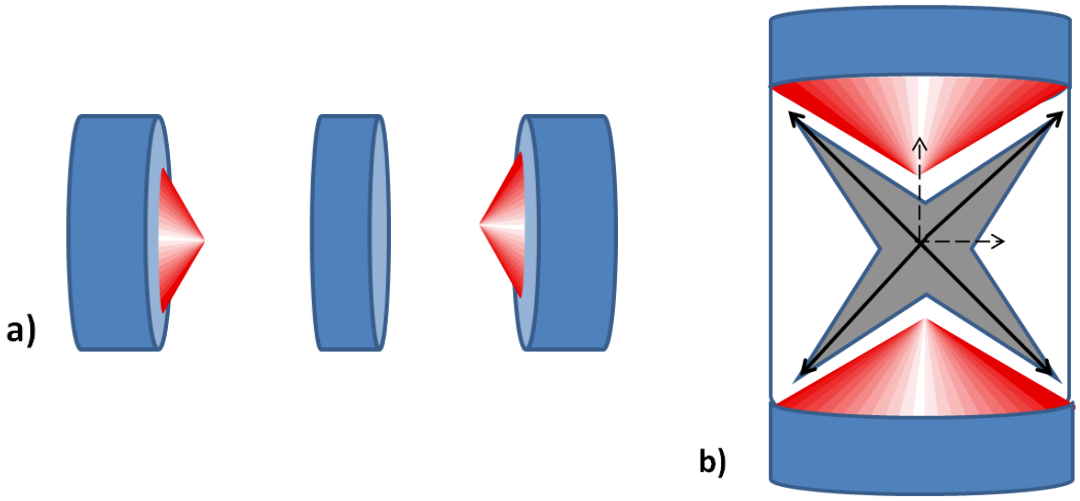

Figure 2.1: Images of (a) an open array of the electrodes which make up a quadrupole ion trap, consisting of two end-cap electrodes with a ring electrode symmetrically between them and (b) a cross section of the electrodes when assembled together creating the ideal geometry with asymptotes represented as black arrows.[55]

The quadrupole ion trap cell is kept at an approximate pressure of 1 mTorr of He buffer gas, which serves to cool the ions and also focus them to the center of the cell.[7, 55, 58] The potential well created by the ion trap electrodes segregates ions in layers, similar to that of liquids with different densities, with the layer of least density corresponding to ions of lowest mass to charge (m/z) ratio. Just as one can decant the top layer of such liquids by tilting the containing vessel, in a similar way, ramping the r.f. amplitude of the ring electrode allows for isolation of particular ions of the desired m/z by selective ejection. As the r.f.

voltage is increased, ions with greater m/z ratios develop unstable trajectories and are ejected through the aperture in the end cap towards a detector. [54] The trajectories of the ions can be characterized by solutions to the Mathieu equations, allowing the ion motion in the quadrupole ion trap to be predicted, as well as whether the trajectory is stable or unstable.[54-55] Equations which include the parameterized coordinates for the formation of a stability diagram based on the Mathieu equations are shown below:

$$q_z = 4eV/mr_0^2\Omega^2 \quad \textbf{[2.1]}$$

$$a_z = -8eU/mr_0^2\Omega^2 \quad \textbf{[2.2]}$$

where V is the r.f. peak voltage, U is the voltage applied to the ring electrode, r_0 is the inscribed radius of the ring electrode, Ω is the angular frequency of the r.f. voltage, m is the mass of the ion, and e is the charge of the ion.[54] The parameters q_z and a_z can then be used to plot a stability diagram.

2.1.3 Collision-Induced Dissociation (CID)

Collision-induced dissociation of an isolated ion species in a quadrupole ion trap is a powerful technique for the determination of ion structures.[55] When a resonant excitation voltage is applied, the ions in the ion trap move away from the center, to a vicinity of higher potential and are accelerated due to the higher potential present in that region, causing an increase in their kinetic energies on the microsecond time-scale. The internal energy of the ions is also increased upon collisions with the buffer gas He atoms, but on the millisecond time-scale.[55] There must however, be a balance between the uptake of kinetic energy and the cumulative and rapid increase of an ion's internal energy. In addition to this, the ejection of

trapped ions and fragment ions must be minimized. Under these conditions, the maximum number of fragment ions can be produced and trapped using CID.

2.1.4 Free Electron Laser (FEL)

The free electron laser is unique because it involves coherent radiation produced as a result of oscillations of free electrons, rather than electrons bound in atoms, molecules, or crystals.[7, 59] The FEL is typically a linear accelerator (LINAC) based light source which can supply high power radiation, while providing the optical characteristics found in conventional laser systems. Relativistic electrons are passed through a periodic magnetic assembly, called an undulator, resulting in the stimulated emission of light.[7, 59] The period of the undulator magnet and the applied magnetic field determine the wavelength of radiation that is emitted, in addition to the energy of the electron beam.[59] The free electron laser is distinct from other lasers because it can be designed to operate at essentially any wavelength.[59-60] The period of the undulator magnet is by definition fixed, but its strength can be varied by altering the distance between the rows of magnets and the FEL is therefore tunable over an extensive range of wavelengths including: X-rays, ultraviolet, visible, infrared, and microwave.[7, 59-60] Most FELs, however, are typically operated in the wavelength range of UV to far-infrared.[60] The free electron laser is also capable of high output power since the electron beam is able to maintain high power without dissipating excess energy in the laser cavity.[59] The FEL is therefore, a high-power and tunable source of coherent radiation, which can provide the necessary photons for IRMPD.[59, 61-63]

Because the IRMPD process normally involves the absorption of tens to hundreds of photons, very powerful lasers are required in order for dissociation to occur. [25] Gas discharge lasers such as the CO_2 laser have been used for IRMPD-type studies, but their use is limited largely because they are not tunable. Optical parametric oscillators (OPO) can also be used for IRMPD-type studies and have the benefit that they are tunable; however, OPO lasers lack the intense power of an FEL. Therefore, it is often ideal for a free electron laser to be used in IRMPD studies.

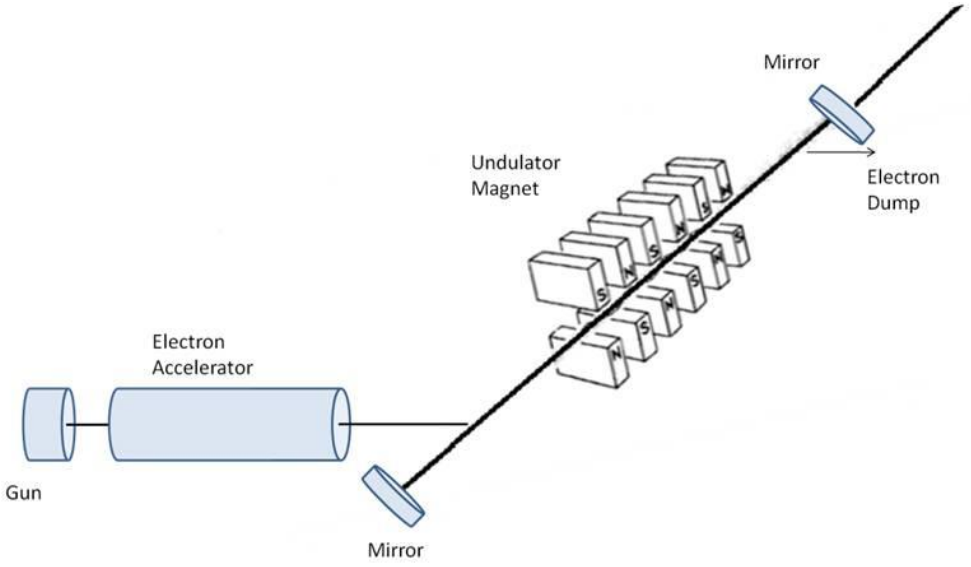

Figure 2.2: A schematic diagram of the components of a free electron laser. The electron accelerator produces relativistic electrons, the undulator magnet causes the electrons to perform a transverse oscillation and emit radiation, and the two mirrors amplify the radiation by stimulated emission.[59]

2.2 Experimental Setup

All IRMPD experiments were performed using the infrared free electron laser (IR-FEL) at the Centre de Laser Infrarouge d'Orsay (CLIO) facility in Orsay, France. The IR-FEL beam was directed into a Bruker Esquire 3000+ ion trap mass spectrometer, equipped

with an electrospray ionization interface. The IR-FEL is created by emission from a 10-50 MeV electron beam which passes through the gap between a set of periodic undulator magnets. By adjusting the undulator gap, the emission photon wavelength is able to be tuned through the mid-infrared range. The undulator is held within a 4.8 m long optical cavity. The laser beam is accumulated in an optical cavity and outcoupling is permitted through a 1-3 mm hole in one of two silver mirrors, each with a diameter of 38 mm.

The work described here involves the use of an electron energy of 46 MeV, which permitted continuous scans over a frequency range of 1000 cm^{-1} to 2000 cm^{-1}. The IR-FEL output consists of a train of 8 μs macropulses, with a repetition rate of 25 Hz. Each macropulse is comprised of approximately 500 micropulses, with a width of a few picoseconds per pulse. For an average IR power of 500 mW, the corresponding micropulse and macropulse energies are about 40 μJ and 20 mJ, respectively.

Sample solutions were prepared (specific details for each species are in the corresponding chapters) and ions were supplied from these solutions using an electrospray ionization interface. The ionic species of interest are then isolated and restricted within the quadrupole ion trap mass spectrometer and the IR-FEL beam is focused and introduced into the center of the ion trap. Following the laser irradiation, consequence mass spectra were recorded and an accumulation of ten spectra were obtained for each wavelength. IRMPD spectra were acquired by scanning the wavelength in steps of ~4 cm^{-1}.

Chapter 3
Computational Methods

3.1 Coupling of Electronic Structure Calculations with Experimental Data

Infrared multiple photon dissociation spectroscopy experiments can yield very detailed information about species in the gas phase and greatly aid in structural elucidation studies; however, though the IRMPD spectrum may contain these details, the information can often be difficult to decipher based exclusively on chemical intuition. Because of this, it can be very useful to use electronic structure calculations in order to assist in structural characterization. IRMPD spectroscopy experiments coupled with electronic structure calculations have proven to be an invaluable method for characterization of gas phase ion structures and energetics.[13, 38, 45-46, 64-65] *GAUSSIAN* 03 or 09 software has been used for all optimization and frequency calculations.[66-67] Electronic structure calculations can provide excellent approximations of thermochemical data and can also be used to generate theoretical infrared (IR) spectra. Theoretical IR spectra for several isomers can be qualitatively compared with the experimental spectrum, and can be used to find an isomer which visibly best matches the experimental spectrum. In other cases, there may be several isomers with similar energetics and spectra, indicating a mixture of isomers, and a combination of their calculated IR spectra might be determined to best match the experimental spectrum. The theoretical spectra can also be useful in designating peak assignments, as GAUSVIEW 5.0 simulates the vibrational modes corresponding to the calculated peaks.[68]

Comparison of the calculated relative energetics of isomers can, in itself, strongly suggest a dominant isomer. Small isomeric differences in structure can have a large impact on the interactions and reactivity of a molecule with itself and its surroundings. The investigation of molecular structures for a given chemical system can provide information regarding isomeric abundances and reactivity in experiment or nature. Assuming that a Boltzmann distribution of internal energies is possessed by the ions, the relative abundances of a mixture of isomers can be predicted by their relative differences in Gibbs free energies. Isomers or complexes which are higher in energy are less likely to form, whereas those with lower energies will be more prevalent. An isomer with a relative Gibbs free energy difference of about +15 kJ/mol (kilojoules per mole) will be present in a ratio of 1:424 with respect to the lowest energy isomer at 298 K. This relationship increases exponentially as the energy difference becomes greater and at approximately 30 kJ/mol, the ratio has increased to over 1:180,000. Given a unimolecular reaction involving species A and B in equilibrium, the following equation can be used in order to determine the above relationship.

$$K = \frac{[B]}{[A]} = e^{\frac{-\Delta G^{\circ}_{298}}{RT}} \qquad \textbf{[3.1]}$$

Because of this, only isomers which are within about 15 kJ/mol of the lowest energy structure are considered to be relevant and accessible in experiment.

3.2 Electronic Structure Calculations

When deciding the appropriate level of theory to use for electronic structure calculations, it is important to consider the combination of basis set and method which will best describe the system of interest. For the content presented in this thesis, a few different levels of theory have been used and will be discussed in the following sections.

Vibrational frequencies, unless otherwise specified, are calculated using the harmonic oscillator approximation to describe the oscillatory motion of the bonds in a species.[69] The harmonic oscillator approximates the potential energy curve for a bond as a parabola. Although the actual curve for potential energy verses stretching of a bond is not entirely in the shape of a parabola, this approximation fits fairly well near the equilibrium bond length since that area of the curve is well approximated by the parabola shape.[70] Calculations performed using this approximation however, have been shown to consistently over-estimate the fundamental frequencies in comparison to experimental values by about 10%.[7, 70] Because the discrepancy between calculated and observed frequencies is fairly constant, scaling factors can be implemented in order to offset the over-approximation of the calculated harmonic frequencies. Scaling factors can be determined using a least squares fit of the scaled harmonic frequencies verses the experimental fundamental frequencies.[71-73] Scaling factors are specific for the level of theory being used, and serve to correct for anharmonicity and other systematic errors.

When the system being calculated is sufficiently small it is sometimes possible to simulate the anharmonic frequencies, though these calculations are exceedingly costly. The anharmonic oscillator approximation fits the potential energy curve more appropriately than

the harmonic oscillator because it has a greater degree of mathematical flexibility and also accounts for the coupling of vibrational modes. A harmonic oscillator approximation is limited in flexibility by the use of a quadratic potential, which does not account for the bond dissociation threshold. In addition, each mode is treated independent of the existence of other(s) and as such, the coupling of modes (anharmonicity) is neglected.[74]

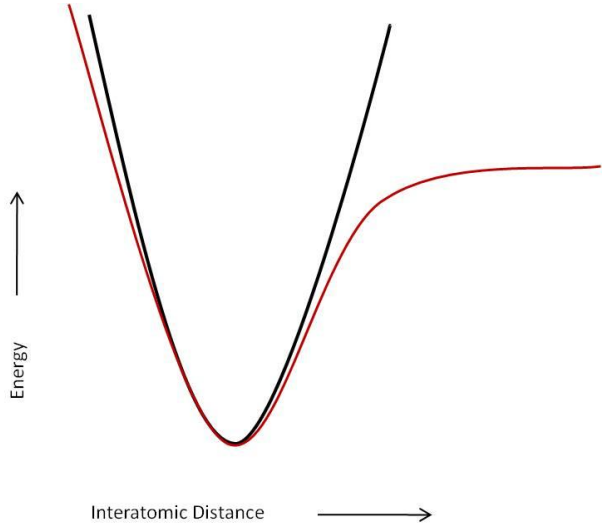

Figure 3.1: A schematic representation of the shape of harmonic and anharmonic oscillators. The parabola used in the harmonic oscillator approximation is shown in black, and the anharmonic oscillator in red.

Single point calculations can be performed in order to better approximate the electronic energy of a species. This step is normally important in order to obtain accurate thermochemical values for a given system. Once a molecular structure is optimized, a frequency calculation is typically performed. Once the optimization and frequency calculations are performed successfully, the electronic energy can be calculated at a higher level of theory, using the pre-optimized geometry of the species. A single point calculation

is based on the energy of electron motion about a fixed field of nuclei and is less resource demanding than an optimization or frequency calculation; thus, higher level methods incorporating electron correlation effects and larger basis sets can be employed.[7]

3.2.1 Methods for Electronic Structure Calculations

Electronic structure calculations aim to supply an approximate solution for the Schrodinger equation. The Schrodinger equation is essential to describing all quantum mechanical problems and its solution for a given system would describe its quantum mechanical behavior.[69] However, the Schrodinger equation cannot be solved without approximations if it is applied to anything larger than a two body system.[69] Therefore, the Born-Oppenheimer approximation can be used in order to simplify and approximate the solution to the Schrodinger equation. The Born-Oppenheimer approximation is based on the idea that the motion of the electrons are much faster than the motion of the nuclei, due to their differences in mass.[69] Based on this concept, the electrons are able to immediately adjust to any change in position of the nuclei and therefore, the electron motion can be determined for a static nuclear arrangement, greatly simplifying the Schrodinger equation.[69]

When electronic structure calculations seek solutions to the Schrodinger equation without the use of any empirical parameters, they are called *ab initio*, which in Latin, means "from the beginning". Ab *initio* methods use the Born-Oppenheimer approximation, but aim to explicitly solve the integrals involved in the Schrodinger equation without additional parameters. MP2 is an example of an *ab* initio method, whereas B3LYP is considered semi-empirical. Semi-empirical methods maintain many of the same fundamentals as *ab initio*

calculations, but replace some integrals with empirical parameters, leading the calculation to obtain results which mimic experimental results.[69] The addition of these parameters, allows semi-empirical methods to handle larger sized molecules, which would otherwise be exceedingly computationally expensive.

3.2.1.1 Hartree-Fock (HF)

Calculations using the Hartree-Fock method are considered the simplest type of ab initio calculation.[70] Although this method was not directly used in any of the calculations discussed in this thesis, components of this method have been incorporated into more modern electronic structure calculations which will be discussed subsequently, and therefore it is important to mention some background on Hartree-Fock. The Hartree-Fock approximation divides up the electron motions into one-electron space wavefunctions and spin functions, which results in organization of the electrons into molecular orbitals.[69] All *ab initio* methods begin with a Hartree-Fock approximation in order to organize the molecular orbitals, but as the level of theory increases in complexity, additional considerations are taken into account, such as, electron correlation.[69]

3.2.1.2 Møller Plesset Perturbation (MPn) Theory: MP2

Before the methods based on density functional theory were as highly developed as they are today, the MP2 method was one of the best ways to gain accuracy while maintaining only a moderate increase in computational cost.[75] This *ab initio* method was often used in "frontier studies" because it is an accurate and reliable model for a wide range of systems, which has

been proven to yield accurate geometry optimizations.[75] Systems with unusual electronic structure can be difficult to model and often require a higher level of theory in order to be accurate, and in the cases where MP2 is inadequate, higher order Møller Plesset Perturbations can be used. In such instances, MP4 successfully addresses many of the problems which MP2 cannot handle and is the common choice for a higher order calculation. MP3 is not often used because it is more computationally costly, but rarely accounts for any of the short comings encountered when using MP2.[75]

The second order Møller-Plesset perturbation (MP2) method is considered to be a relatively high level of theory which can adequately describe the electronic and thermochemical properties of a wide variety of systems. The MP2(full) parameter can be included to correlate the core and valence electrons rather than exclusively the valence electrons. The theory behind the MP2 method begins by considering a small perturbation to the Hartree-Fock Hamiltonian scaled by a dimensionless parameter.[7] The zeroth-order wave function is then the unperturbed operator and the perturbation is the correlation potential. If these are then expressed as an infinite series, they can be substituted into the time-independent Schrodinger equation.[76]

3.2.1.3 Density Functional Theory (DFT): B3LYP

Density functional theory methods have dramatically grown in popularity over the recent years due to the fact that they are capable of achieving significantly greater accuracy than Hartree-Fock calculations with only a very slight increase in computational cost.[75] DFT is a semi-empirical method and is capable of this notable accuracy to cost ratio because it

includes electron correlation effects in a much less computationally demanding manner than traditional correlated methods.[75] The electron correlation effects are calculated using general functionals of the electron density and are separated into several components: kinetic energy, electron-nuclear interaction, the Coulomb repulsion, and an exchange-correlation term which are calculated separately. Hybrid functionals of the DFT method also exist and have been shown to be superior to the traditional functionals because they have greater accuracy with no additional cost.[75, 77] A hybrid functional incorporates a portion of exact exchange from Hartree-Fock theory with exchange and electron correlation from other sources.[78] An example of a hybrid DFT functional is the B3LYP (Becke 3-Parameter, Lee, Yang and Parr) method, which is the outcome of mixing Hartree-Fock theory and local density functional theory. This hybrid method has been used extensively in the research presented in this thesis, and has been proven to show good performance for a very large range of chemical systems and properties.[64, 79-80] In fact, it has become the most popular DFT method to this day and has been called the "workhorse of quantum chemistry".[80-81] The B3LYP method has proven, in a variety of applications, to be more efficient and accurate than MP2, especially with respect to the calculation of infrared vibrational spectra.[7, 81]

3.2.1.4 Density Functional Theory: B2PLYP

The B2PLYP method is considered a double-hybrid density functional and is based on the B3LYP method discussed previously, but with a perturbative second-order correlation component (from MP2) included.[82] It therefore has electron correlation from local density functional theory, Hartree-Fock exchange, and a second-order perturbation correlation

constituent. Thus, it acquires its name B2PLYP by the number of parameters and the order of perturbation being "2", "P" represents perturbative correlation, and "LYP" denotes the LYP density functional.[82] During its initial testing, it was found to have mean absolute deviations smaller than any of the other density functionals and because of this, the creator boldly stated that it could be the best general purpose density functional for molecules.[82] In addition to this, the B2PLYP method has been declared to be a very robust and efficient method which could be used practically in a wide range of applications.[82] Although, B2PLYP is a fairly new method, it has been found to be a competitive alternative to B3LYP and was found to perform as well or better in most test sets, with only a moderate increase in computational demand.[80]

3.2.2 Basis Sets for Electronic Structure Calculations

The approximate total electronic wavefunction of a system is a combination of the orbitals which can be mathematically described using a basis set. Larger basis sets are able to better approximate the orbitals in a system because they have parameters that provide the electrons with more freedom to move around in space. The size of the basis set required for the study of a given system greatly depends upon the atoms that make up the species, as well as the complexity of the interactions. Standard basis sets employ linear combinations of Gaussian functions to form the orbitals and are often named based on the number and type of basis functions they use. A basis set involves a group of basis functions for each atom in a species in order to approximate the orbitals, which are also based on a linear combination of Gaussian functions, and are individually called primitives.[75]

There are a wide variety of basis sets available which differ in size and the number of restrictions placed on the locations of the electrons in space. Minimal basis sets are small and use only the minimal number of basis functions required for each atom, calculated using fixed-size atomic-type orbitals.[75] An example of a minimal basis set is STO-3G which is a Slater-type orbital that uses three Gaussian primitives per basis function. Another type of basis set is the split valence basis set in which the number of basis functions per atom is increased and certain orbitals differ in size.[75] The notation for split-valence basis sets was created by John Pople, and therefore, they are also often referred to as Pople-style basis sets. An example of a split valence basis set would be 6-311G, which has six sets of basis functions for the core electrons and three sets for the valence, which includes three basis functions for the first and one for each of the other two sets.

Another way in which a basis set can increase in size is by adding polarization parameters that give the orbitals freedom to change in shape. Polarized basis sets remove limitations on shape by adding orbitals with angular momentum in excess of what is required for the ground state.[75] Polarization parameters can allow d functions on carbon atoms, f functions on transition metals, and can also be used to add p functions to hydrogen atoms when needed. An example of a polarized basis set is 6-311G(d,p), in which the "(d,p)" parameter adds d functions to heavy atoms and p functions to hydrogen atoms. This parameter is also often indicated by either * or ** for the addition of d functions and the addition of both d and p functions, respectively. In addition, a basis set such as 6-31G(2d) would indicate that two d functions are added per heavy atom.

Diffuse functions can also be added to a basis set in order to allow the orbitals to reside in a larger area of space. This is an important parameter for systems in which the electrons are located somewhat farther away from the nucleus, as found in molecules with lone pairs, anions, excited states, etc.[75] Basis sets with diffuse functions include 6-311+G(d,p) and 6-311++G(d,p) in which the single + indicates the addition of diffuse functions on the heavy atoms, and the ++ corresponds to diffuse functions on both the heavy atoms and the hydrogen atoms.

3.2.2.1 Pople-Style Basis sets: Specifically, 6-311+G(d,p)

The 6-311+G(d,p) basis set is a split valance basis set that is triple zeta with 6 sets of basis functions for the core electrons, and three sets for the valence, including 3 basis functions for the first and one for each of the other two sets. In addition, this basis set has polarization parameters that place d functions on the heavy atoms and p functions on the hydrogen atoms. There are also diffuse functions on the heavy atoms.

This basis set was used in combination with the B3LYP method for the optimization and frequency calculations performed in Chapters 5 and 6. For both projects, the optimization and frequency calculations were performed at the B3LYP/6-311+G(d,p) level of theory with a scaling factor of 0.9679.[71, 83-88] This level of theory has been shown to provide superior calculated infrared vibrational spectra, in addition to having an excellent balance between accuracy and cost.[75, 79, 81] Diffuse functions were not included on the hydrogen atoms as it has been shown that this rarely leads to a significant difference in accuracy.[75]

3.2.2.2 Correlation Consistent, Polarized Valence, x-Zeta Basis sets: Specifically, aug-cc-pVTZ

The aug-cc-pVTZ basis set is augmented with diffuse functions on both the heavy atoms and the hydrogen atoms, which allows for the size of the orbital to increase as needed in the calculation. This parameter is indicated by "aug" in the name of the basis set. The abbreviation "cc-pVTZ" stands for correlation-consistent polarized valence triple zeta. As the zeta factor increases, the calculations become increasingly accurate as well as increasingly computationally demanding. Triple zeta forms all molecular orbitals from linear combinations of three sizes of functions for each orbital type. Correlation consistent basis sets add subsequent shells of functions to a core set of atomic Hartree-Fock functions and each shell contributes approximately the same amount of correlation energy.[89]

The aug-cc-pVTZ basis set was used in combination with the MP2 method for the calculations in Chapter 4 and in combination with the B2PLYP method for the single point calculations in Chapter 5 on 5-fluorocytosine. This basis set is fairly large and therefore was chosen with the MP2 method because it would lead to very accurate results and provide reliable thermochemical data. For calculations in Chapter 4, the MP2(full)/aug-cc-pVTZ level of theory was used with a scaling factor of 0.969.[90-91] The "full" parameter was included in order to include the core electrons in the correlation energy.

In Chapter 5, this basis set was also chosen for single point calculations with the B2PLYP method because in addition to being well fitted for the systems being studied, it is recommended for use with the new double hybrid functional since the parameters in the functional were fit using this basis set.[92]

3.2.3 Conclusions

The calculations in Chapter 4 were performed using MP2(full)/aug-cc-pVTZ because this level of theory has been found to provide excellent optimization geometries and generally be quite accurate.[75, 93] It is also a reasonably high level of theory and since uracil and 5-fluorouracil are fairly rigid molecules, and the cluster molecules are small enough, the balance between computational cost and accuracy could favour accuracy. Geometry optimization and frequency calculations for the subsequent studies involving 5-fluorocytosine and ferulic acid, however, were performed at the B3LYP/6-311+G(d,p) level of theory because it has proven to provide an accurate vibrational analysis, in addition to its excellent compromise between accuracy and cost.[79] All in all, the best level of theory to use for a certain system or type of systems is a learning process. In the case of the studies presented in this thesis, all systems involve relatively small biological molecules in the gas phase. In the opinion of the author, the B3LYP/6-311+G(d,p) level of theory with the scaling factor of 0.9679, has proven itself to be superior for the calculation of energetics and infrared vibrational spectra in these types of systems. This has been deduced primarily because of the exceptional matches that have been obtained between experimental and calculated IR spectra and also because the calculations at the MP2(full)/aug-cc-pVTZ level of theory proved to be much higher in computational cost, and in some instances failed to converge. The coupling of IRMPD spectroscopy experiments with electronic structure calculations at the B3LYP/6-311+G(d,p) level of theory has been reported to give excellent results in the literature as well.[13, 38, 64, 80, 94]

Chapter 4
Characterization of Uracil and 5-Fluorouracil in the Gas Phase by IRMPD and Electronic Structure Calculations

4.1 Introduction

Uracil is one of the five nucleic acid bases, and is classified as a pyrimidine along with cytosine and thymine. Uracil is a component of RNA that base pairs with adenine and in DNA is replaced by thymine.[95] Uracil can be fluorinated at position five to form 5-fluorouracil (5-FU), which is commonly used today in the pharmaceutical industry as an anti-cancer drug. 5-Fluorouracil was proposed and developed by rational drug design as a potential anti-cancer drug in 1957 and has since then become one of the most useful antitumor agents.[96] 5-Fluorouracil has been used for over forty years in the battle against colorectal, pancreatic, skin, and certain aggressive forms of breast cancer.[97-98] The drug has several modes of action in the body, the principle mode being a thymidylate synthase inhibitor; however, there are many additional ways in which this drug acts that are still not fully understood.[97-98] In the body, 5-fluorouracil can also be incorporated into RNA in place of uracil, leading to problems in the affected RNA strands.[98-99] No matter the method of action taking place, disruption of DNA synthesis is the ultimate outcome, leading to its anti-cancer activity.

Characterization of the structures and energetics of these species on their own and in clusters with various small molecules, will allow for a better understanding of their

interactions with common functional groups found biologically. Because there are several mechanisms of action relating to 5-fluorouracil which are not yet understood, knowledge of structure and functionality will allow for a deeper understanding of how this drug works and potentially how it could be enhanced in the future.

4.2 Methods

4.2.1 IRMPD of Uracil and 5-Fluorouracil

IRMPD spectroscopy experiments were attempted as described in Chapter 2 in order to characterize uracil and 5-FU. Solutions were prepared by mixing the corresponding solid in an 80:20 mixture of acetonitrile and water. A small amount of ammonium hydroxide was added in order to aid in deprotonation where appropriate. These species however, could not be studied by IRMPD as we were unable to fragment them. It is suggested that the IRMPD process was not efficient enough to overcome the lowest-energy dissociation threshold of the species. A similar situation was encountered by Fridgen and coworkers when performing IRMPD experiments on $[PbGly\text{-}H]^+$.[100]

4.2.2 Electronic Structure Calculations

Geometry optimization and frequency calculations have been performed on uracil and 5-fluorouracil at the MP2(full)/aug-cc-pVTZ level of theory with a scaling factor of 0.969, as described in detail previously. The nosymm specification was included in order to ensure that no assumptions were made regarding symmetry in the molecule.

For both uracil and 5-fluorouracil, optimization calculations were performed on neutral isomers and deprotonated isomers. The relevant deprotonated species were then clustered with water, methanol, ammonia, and methylamine. These small molecules were chosen in order to provide model interactions for some common functional groups found biologically. Water illustrates an interaction with itself and methanol further illustrates this interaction with an R-OH group. Ammonia and methylamine contain NH_3 and R-NH_2 groups respectively, which provide a model for biological interactions involving nitrogen.

4.3 Structures and Energetics of Uracil and 5-Fluorouracil

4.3.1 Characterization of Uracil and 5-Fluorouracil

Both uracil and 5-fluorouracil have been characterized by electronic structure calculations. All relevant isomers which have been optimized for uracil, 5-fluorouracil, and their analogs are provided in Appendix A, along with their relative Gibbs free energies (298 K). In the following section only 5-fluorouracil will be discussed in detail since similar results have been obtained for both uracil and 5-FU.

4.3.2 Neutral 5-Fluorouracil

Neutral isomers of 5-fluorouracil have been optimized and are shown below in Figure 4.1. The relative Gibbs free energies (298 K) of these species indicate a single energetically relevant neutral isomer, FU-Neutral 01. FU-Neutral 01 is a diketo structure with a proton on

each of the nitrogen atoms. The other neutral isomers are significantly higher in energy than FU-Neutral 01 and will therefore not be considered experimentally accessible, as they would likely be present in a very small ratio relative to FU-Neutral 01.

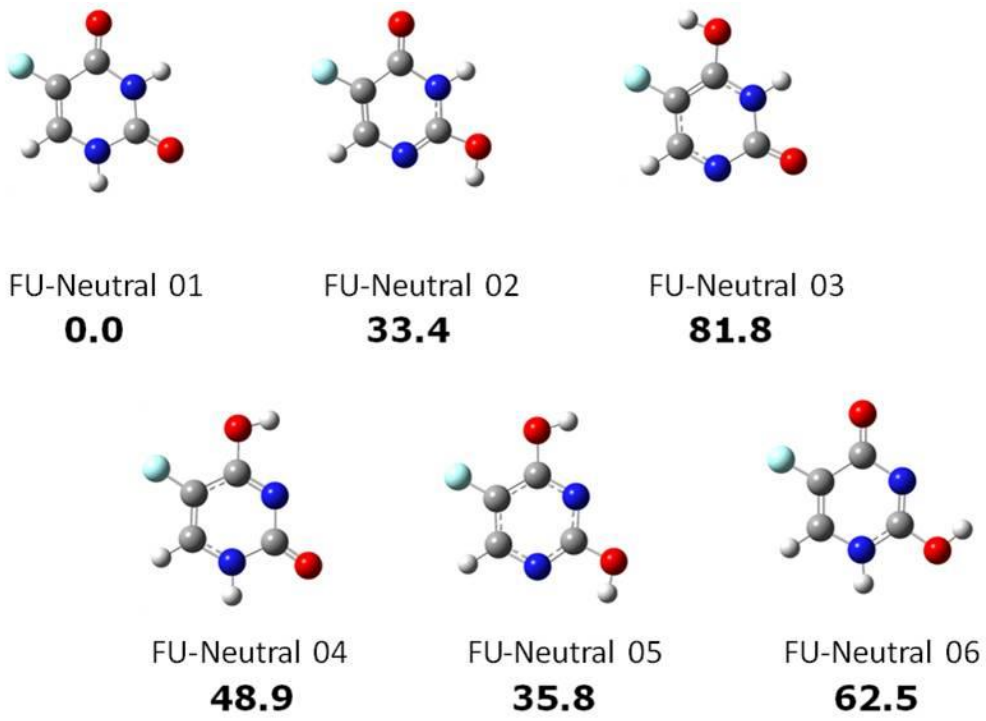

Figure 4.1: Calculated neutral isomers of 5-fluorouracil with relative Gibbs free energies (298 K) in kJ/mol.

4.3.3 Deprotonated 5-Fluorouracil

Based on energetic considerations, FU-Neutral 01 should be the principle isomer that is observed experimentally; therefore, only deprotonated forms of this isomer have been considered. Isomers of deprotonated 5-FU have been optimized and are shown below in

Figure 4.2. Deprotonation of FU-Neutral 01 can occur by removal of either of the protons on the nitrogen atoms. Removal of the proton at site A, on the nitrogen found between the two carbonyl oxygens, has been calculated to be much less favourable than removal of the proton at site B.

Because uracil is an important biological molecule, its acidity in the gas phase has been established previously and the nitrogen at site B is recognized as the most acidic site, which is in agreement with the calculations performed for uracil, and remains true for the calculations of 5-fluorouracil.[101-102] Biologically it is the nitrogen at site B where uracil becomes covalently bonded to a carbon of the ribose sugar in RNA.[102] If the addition of fluorine had altered the most favourable site of deprotonation, it could have an effect on the covalent bond which is required to form with ribose at this site, in order to be incorporated into RNA. The incorporation of 5-fluorouracil in place of uracil in RNA is one of the primary mechanisms in which 5-FU is an anti-tumor agent.

Because of the significant difference in energy between the two deprotonated isomers, FU-01-H2 will be considered to be the dominant deprotonated isomer, and will be considered for involvement in the subsequent cluster interactions.

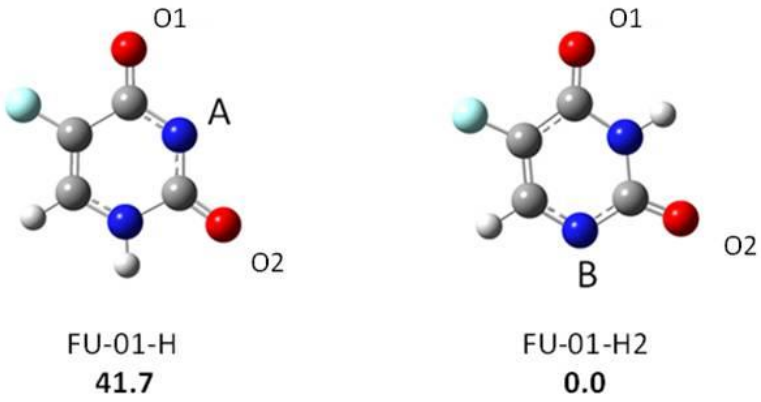

Figure 4.2: Calculated deprotonated isomers of 5-fluororacil. Relative Gibbs free energies (298 K) are shown in kJ/mol. The carbonyl oxygens are labeled for reference in the following sections.

4.3.4 Deprotonated 5-Fluorouracil Clustered with Water

Calculations have been performed on deprotonated 5-FU clustered with water at a variety of different sites and orientations. The calculated lowest energy isomer for the cluster of deprotonated 5-fluorouracil with water is shown in Figure 4.3. Based on the relative energetics of the calculated isomers the lowest energy interaction, found in isomer FU-H_2Oa, occurs at the site of deprotonation. In this isomer, water interacts with deprotonated 5-fluorouracil in a bidentate interaction between the deprotonated nitrogen and the adjacent carbonyl oxygen O2. In the second lowest energy calculated isomer, water is involved in a monodentate interaction with the carbonyl oxygen adjacent to the site of deprotonation, resulting in a higher relative Gibbs free energy (298 K) by 3.4 kJ/mol. Five calculated isomers have relative energetics within 15 kJ/mol of the lowest energy isomer (Appendix A) and therefore, based on the relative energetics, FU-H_2Oa should be the most abundant

isomer, but a mixture of the other relevant isomers would likely be present in experiment as well.

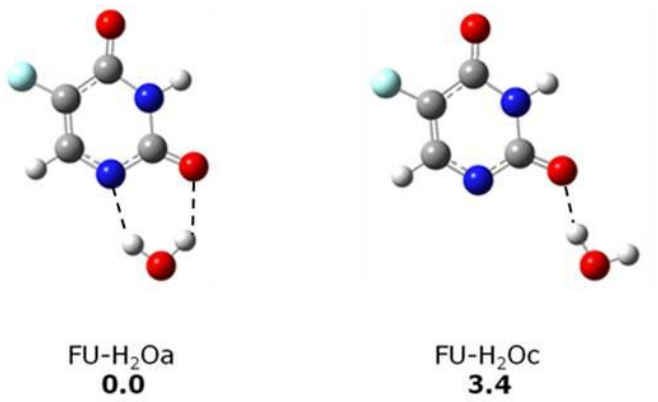

Figure 4.3: The calculated lowest energy isomers for deprotonated 5-fluorouracil clustered with water. Relative Gibbs free energies (298 K) are shown in kJ/mol.

4.3.5 Deprotonated 5-Fluorouracil Clustered with Methanol

Deprotonated 5-fluorouracil has also been clustered with methanol in order to model an interaction with an R-OH group. Cluster interactions between deprotonated 5-FU and methanol have been calculated at a variety of different sites and orientations. The calculated lowest energy isomer, FU-MeOHa, is shown in Figure 4.4 below, and contains an ionic hydrogen bond interaction between methanol and the deprotonated nitrogen of 5-FU. There are four low energy isomers that have been calculated for this cluster (Appendix A); however, the next lowest energy isomer is 5.3 kJ/mol higher in energy. The relative Gibbs free energies (298 K) of the calculated isomers indicate that FU-MeOHa will be the dominant isomer among a mixture of the other calculated isomers.

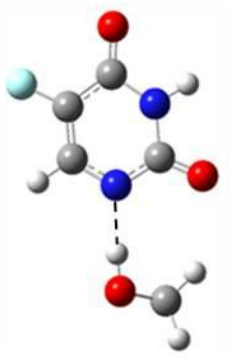

FU-MeOHa

Figure 4.4: The calculated lowest energy isomer of deprotonated 5-fluorouracil clustered with methanol.

4.3.6 Deprotonated Uracil Clustered with Ammonia

Interactions of deprotonated 5-fluorouracil and ammonia have been calculated and the lowest energy isomer is shown in Figure 4.5. The relative energetics of the other calculated isomers are shown in Appendix A, and indicate that FU-NH_3c will be the dominant isomer. This species includes a bidentate interaction with ammonia at the site of deprotonation, between the deprotonated nitrogen and the adjacent carbonyl oxygen O2. The next lowest energy isomer, with a relative energy of 2.6 kJ/mol, also involves a bidentate interaction between the deprotonated nitrogen and carbonyl oxygen O2, but ammonia is in a different spatial configuration, forming a diastereomer of FU-NH_3c. Because of the small difference in relative Gibbs free energy (298 K) between FU-NH_3c and FU-NH_3a these two isomers will likely be present in similar abundance; however, it is probable that a mixture of the other low energy isomers will be present in experiment as well.

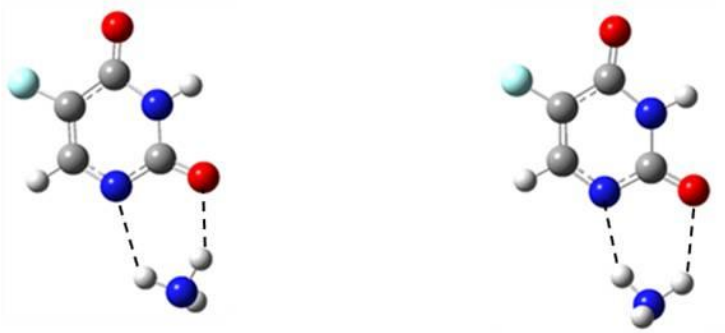

Figure 4.5: The calculated lowest energy cluster of ammonia with deprotonated 5-fluorouracil. Relative Gibbs free energies (298 K) are shown in kJ/mol.

4.3.7 Deprotonated 5-Fluorouracil Clustered with Methylamine

Calculations of deprotonated 5-fluorouracil clustered with methylamine have also been performed. The two lowest energy calculated isomers for this species are shown in Figure 4.6 below. The lowest energy isomer, FU-$MeNH_2$a involves a bidentate interaction at the site of deprotonation between the deprotonated nitrogen and carbonyl oxygen O2. However, methylamine also forms a different bidentate interaction in isomer FU-$MeNH_2$c, which is only 1.6 kJ/mol higher in relative Gibbs free energy (298 K). Five calculated low energy isomers for the cluster of deprotonated 5-FU with methylamine are within 10 kJ/mol of the lowest energy isomer, FU-$MeNH_2$a, and therefore will likely be present to some degree in experiment (Appendix A); however, FU-$MeNH_2$a and FU-$MeNH_2$c are expected to be the most abundant.

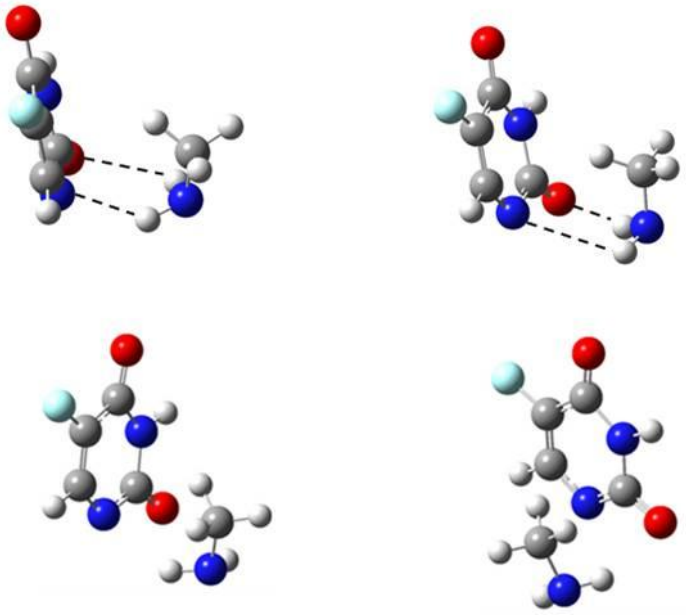

Figure 4.6: The two calculated lowest energy isomers for the cluster of methylamine and deprotonated 5-fluorouracil. Above each isomer is an additional image further depicting the ionic hydrogen bond interactions found in that structure. Relative Gibbs free energies (298 K) are reported in kJ/mol.

4.4 Conclusions

Calculations have been performed on uracil and 5-fluorouracil to obtain lowest energy isomers of the neutrals and deprotonated species, in addition to interactions involving deprotonated uracil clustered with either water, methanol, ammonia, or methylamine. For each cluster interaction calculated lowest energy isomer(s) have been determined; however, due to the number of isomers within 15 kJ/mol it is likely that in each case, a mixture of isomers would be observed in experiment. Bidentate interactions have formed whenever

possible and are present in the lowest energy isomers of clusters involving water, ammonia, and methylamine. It is unfortunate that the IRMPD spectroscopy experiments were unsuccessful, as they may have greatly helped define the dominant species for each cluster. Nevertheless, with the calculated relative energetics as they are, it is likely that each of the lowest energy isomer(s) would have been dominant among a mixture of the other low energy isomers.

Chapter 5
Characterization of 5-Fluorocytosine and Related Analogs in the Gas Phase by IRMPD and Electronic Structure Calculations

5.1 Introduction

The pyrimidine 5-fluorocytosine (5-FC) is a fluorinated analog of the DNA nucleobase cytosine. 5-FC, as a pharmaceutical, is sometimes referred to as Flucytosine or is sold as the drug Ancobon®, and is the only antifungal agent available that acts as an antimetabolite drug.[9] Its mechanism of action has been debated over the years and is thought to be a combination of two or more processes which interfere with pyrimidine metabolism.[103-105] Conversion of 5-fluorocytosine to 5-fluorouracil can occur within the fungal cells.[106] There are two main mechanisms proposed, first, an analog of 5-fluorouracil functionally inhibits the enzyme thymidylate synthase, the sole source of de novo synthesis of thymine in the body.[107] Secondly, another possible mechanism involves a 5-fluorouracil analog being incorporated in place of uridylic acid in fungal RNA, disrupting subsequent protein and carbohydrate synthesis.[103]

5-Fluorocytosine has also been used in recent cancer research involving suicide gene therapy, in what is considered an experimental approach to tumor cell death. This process involves 5-fluorocytosine being activated to 5-fluorouracil inside the tumor, which

subsequently inhibits thymidylate synthase, leading to reduced DNA synthesis and consequently a decrease in tumor growth.[108]

5.2 Methods

5-Fluorocytosine has been characterized using infrared multiple photon dissociation (IRMPD) spectroscopy as described in Chapter 2. Solutions of 5-fluorocytosine were prepared by mixing solid 5-fluorocytosine in an 80:20 mixture of acetonitrile and water. For the cationic dimer experiments involving protonated 5-FC, a small amount of formic acid was added. Deprotonated 5-FC was produced for the anionic dimer experiments by adding a small amount of ammonium hydroxide. To solutions prepared for the 5-FC clusters with chloride and trimethylammonium, NaCl and trimethylammonium chloride were added, respectively.

As described in Chapter 3, all geometry optimization and frequency calculations were performed at the B3LYP/6-311+G(d,p) level of theory, with the harmonic frequencies scaled by a factor of 0.9679.[71, 86, 109-110] Single point calculations were performed on relevant low energy isomers for a better approximation of the electronic energy (B2PLYP/aug-cc-pVTZ). Anharmonic frequencies have been calculated at the B3LYP/6-311+G(d,p) level of theory for the 5-fluorocytosine cluster with chloride.

5.3 Structures and Energetics of 5-Fluorocytosine and Related Analogs

5.3.1 Neutral 5-Fluorocytosine

Four neutral isomers of 5-fluorocytosine have been optimized and are shown in Figure 5.1 below. For reference in the following sections, neutral isomers will be referred to as FC-Neutral 01, 02, 03, or 04 and will be referring to those species shown here. Due to the significantly higher relative Gibbs free energy (298 K) of Neutral 02, it can generally be considered to be negligible under the experimental conditions. However, for subsequent optimization calculations, FC-Neutral 02 was still considered, where appropriate, for completeness, but the relative energetics containing Neutral 02 were always found to be quite high.

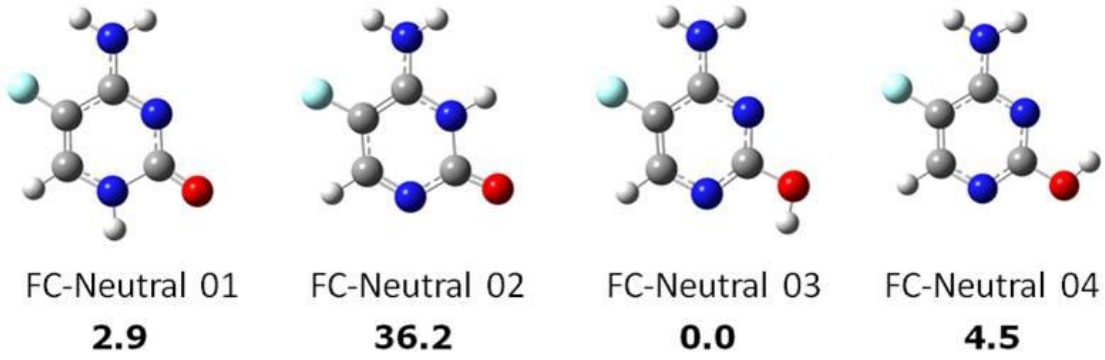

Figure 5.1: Neutral isomers of 5-fluorocytosine. Relative Gibbs free energies (298 K) are shown in kJ/mol.

5.3.2 5-Fluorocytosine Clusters with Trimethylammonium

Trimethylammonium (TMA) has been chosen to cluster with 5-fluorocytosine, as it may provide a model for cationic interactions with 5-FC which exist in biological systems. Both planar and non-planar isomers of the trimethylammonium-5-FC cluster have been considered. A set of calculated lowest energy isomers are shown in Figure 5.2 below.

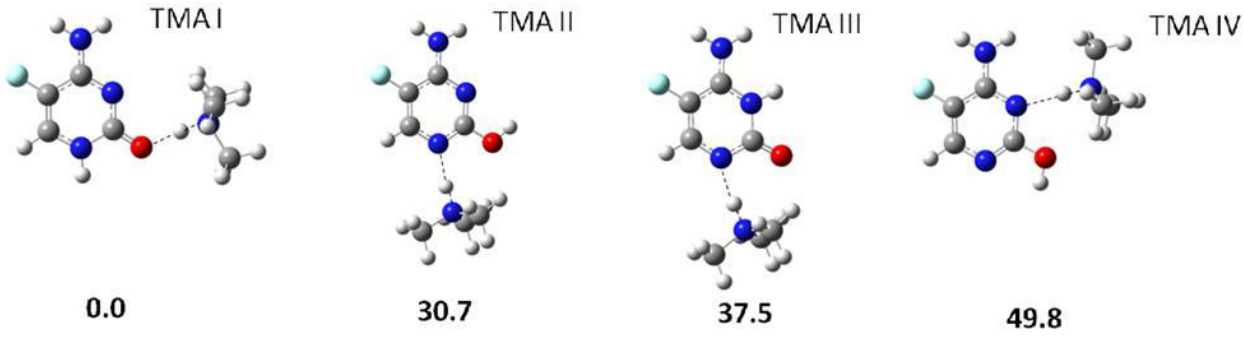

Figure 5.2: The lowest energy calculated isomers for the trimethylammonium-5-FC cluster. Relative Gibbs free energies (298 K) are shown in kJ/mol.

Comparison of the calculated relative Gibbs free energies (298 K) of the isomers shown in Figure 5.2 suggests that the dominant isomer should exist with the structure of TMA-I. TMA-I is bound by an ionic hydrogen bond formed between trimethylammonium and the carbonyl oxygen of 5-fluorocytosine. The proton involved in the ionic hydrogen bond of this species lies more closely to trimethylamine than 5-fluorocytosine since the calculated bond lengths of O1 to H1 and H1 to N3 are 1.59 Å and 1.07 Å, respectively. The proton affinity for 5-fluorocytosine has been calculated to be 941 kJ/mol (B2PLYP/aug-cc-pVTZ//B3LYP/6-311+G(d,p)) and the established proton affinity for trimethylamine is 948.9

kJ/mol.[111] During the original optimization procedures, starting structures of several additional isomers converged through proton transfer tautomerism, to isomer TMA-I, the lowest energy isomer. All other calculated species for the trimethylammonium-5-FC cluster have relative Gibbs free energies (298 K) in excess of 30 kJ/mol in comparison to TMA-I, and are therefore considered to be negligible under the experimental conditions. Values of ΔG° (298 K) for the formation of each of the isomers in Figure 5.2 is shown in Table 5.1 below. These values are based on formation as follows:

$$TMA^+ + 5\text{-FC} \rightarrow [TMA\text{-}5\text{-}FC]^+ \qquad \textbf{[5.1]}$$

Table 5.1: Thermochemical values (298 K) for the formation of several trimethylammonium-5-FC clusters. Values have been calculated at the B2PLYP/aug-cc-pVTZ//B3LYP/6-311+G(d,p) level of theory and are reported in kJ/mol for ΔG° and ΔH°, and in J/mol K for ΔS°.

TMA Isomer	ΔH°	ΔS°	ΔG°
I	-140	-139	-98.7
II	-113	146	-69.3
III	-140	-149	-95.5
IV	-86.5	-133	-46.8

Calculated harmonic spectra for TMA isomers I, II, III, and IV are shown in comparison with the experimental spectrum in Figure 5.4. The experimental spectrum has significant peaks arise at 1621 and 1660 cm^{-1}, which are revealed by computational analysis as a R-C=O---H-N^+-R_3 carbonyl stretch in asymmetric motion with the proton of

trimethylammonium. These peaks are found to match well in the calculated TMA-I and experimental spectrum, strongly suggesting that TMA-I is the species being observed in experiment. An image of TMA-I is shown in Figure 5.3 with the relevant atoms labeled for reference.

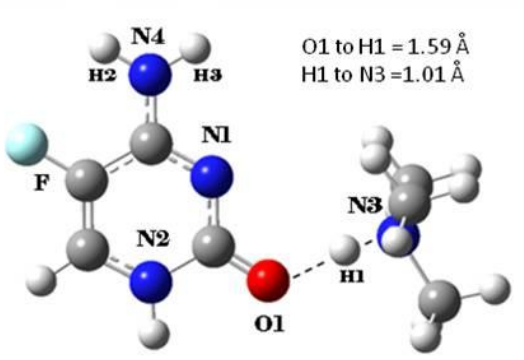

Figure 5.3: The lowest energy trimethylammonium-5-FC isomer, TMA-I, with relevant atoms labeled. Ionic hydrogen bond lengths are stated in Angstroms (Å). For the purpose of reference, the same atom labels will be used when describing other isomers as well, where appropriate.

Calculated vibrational spectra corresponding to the higher energy isomers, TMA-II, -III, and –IV have peaks indicating alternate sites of interaction between 5-FC and trimethylammonium and do not approximate the experimental spectrum as closely. TMA-II has a large peak at 1478 cm^{-1} from the H1 proton rocking between N3 and N2 and this peak is red-shifted in comparison to peaks found in the experimental spectrum. A peak at 1270 cm^{-1} in the calculated TMA-III spectrum corresponds to H1 rocking between trimethylamine and N2 of 5-FC and less closely approximates peaks in the experimental spectrum. Finally, the calculated spectrum of TMA-IV has a larger peak at 1093 cm^{-1} compared to the other

calculated spectra, which corresponds to NH_2 rocking in addition to the rocking of the O1 hydroxyl group found in this isomer. There is also a peak at 1460 cm^{-1}, which is characteristic of the site of interaction, arising from the H1 proton rocking between N1 on 5-FC and N3 on trimethylammonium. The calculated TMA-I spectrum, however, is found to match the experimental spectrum exceptionally well. Therefore, from analysis of both spectra and energetics, TMA-I is suggested to be the dominant isomer for the trimethylammonium-5-FC cluster, with the site of interaction occurring between the oxygen atom of 5-FC and the nitrogen atom of trimethylammonium.

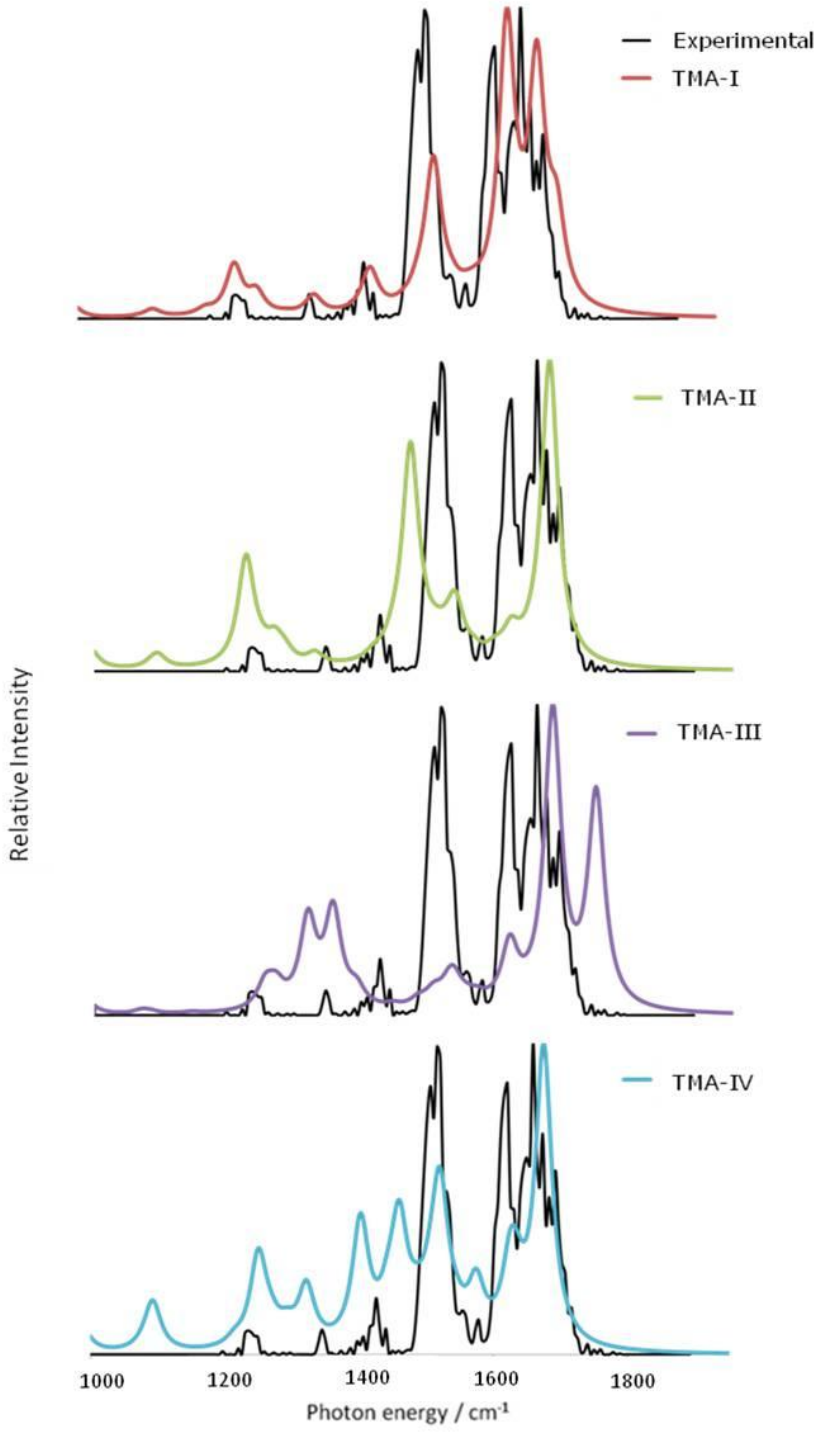

Figure 5.4: A comparison of the harmonic calculated spectra for several isomers of the trimethylammonium-5-FC cluster with the experimental spectrum. Harmonic spectra were calculated at the B3LYP/6-311+G(d,p) level of theory with a scaling factor of 0.9679.

5.3.3 5-Fluorocytosine Clusters with Chloride

5-Fluorocytosine has been chosen to cluster with chloride as it may provide a model for anionic interactions with 5-FC which exist in biological systems. Calculations of chloride interacting with a variety of different sites on each energetically relevant neutral 5-FC isomer were calculated. Based on relative Gibbs free energies (298 K), there appears to be five isomers which can be considered experimentally accessible. Optimized isomers of the chloride-5-FC cluster are shown in Figure 5.5 along with their relative Gibbs free energies (298 K).

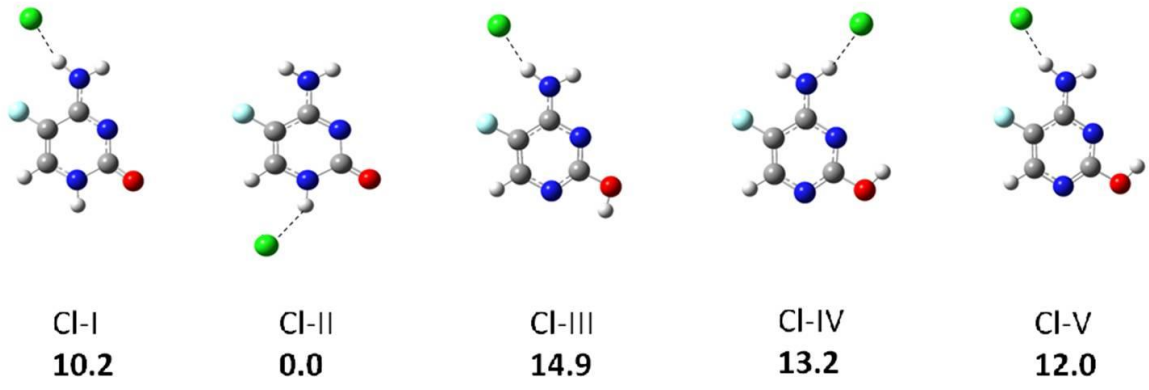

Figure 5.5: Structures and relative Gibbs free energies (298 K) for several isomers of the chloride-5-FC cluster. Relative Gibbs free energies (298 K) are reported in kJ/mol.

Calculated thermochemical values (298 K) for the formation of several chloride-5-FC isomers are shown in Table 5.2. These values are based on formation of the 5-fluorocytosine cluster with chloride as follows:

$$Cl^- + 5\text{-FC} \rightarrow [Cl\text{-}5\text{-FC}]^- \qquad \textbf{[5.2]}$$

Table 5.2: Thermochemical values (298 K) for the formation of several chloride-5-FC isomers. Values have been calculated at the B2PLYP/aug-cc-pVTZ//B3LYP/6-311+G(d,p) level of theory and are reported in kJ/mol for ΔH° and ΔG° and in J/mol K for ΔS°.

Chloride Isomer	ΔH°	ΔS°	ΔG°
I	-95.3	-93.3	-67.5
II	-107	-99.5	-77.1
III	-87.3	-94.9	-59.0
IV	-91.4	-89.8	-64.7
V	-92.1	-93.3	-65.2

The lowest relative energy isomer is Cl-II and is shown in Figure 5.7 with relevant atoms labeled. Isomer Cl-II situates the chloride ion furthest away from the electronegative heteroatoms in the molecule and contains an ionic hydrogen bond interaction between the chloride ion and H1 with a bond length of 2.19 Å. In the other four relevant structures, chloride is in association with the amino group of 5-FC, and this difference consequently yields a unique vibrational spectrum for Cl-II.

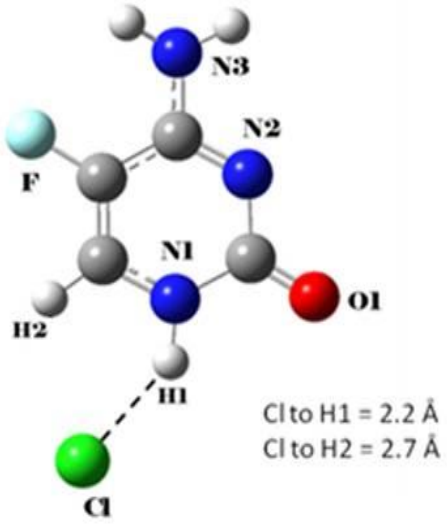

Figure 5.6: The lowest energy chloride-5-FC isomer, Cl-II, with relevant atoms labeled. For the purpose of reference, the same atom labels will be used when describing other isomers as well. Ionic hydrogen bonds are represented as black dotted lines and bond lengths are reported in Angstroms (Å).

The calculated spectrum for each of the five lowest energy isomers is shown in comparison with the experimental spectrum in Figure 5.8 below. For isomers Cl-V, -IV, and –III, O1 is present in the enol form and has chloride associating with the amino group of 5-FC. There are no carbonyl peaks in the spectra corresponding to these isomers; however, each contains a relatively red-shifted peak in the region of approximately 1700 cm^{-1}, present from Cl---NH_2 scissoring. Each of the related spectra for these isomers also contains a peak at approximately 1500 cm^{-1}, representing an O1-H rocking motion within the enol functionality. In addition, Cl-V does not account for a peak found experimentally at 1316 cm^{-1}, which likely corresponds to the in-plane rocking of H1 in association with chloride. The calculated spectrum of the lowest energy isomer, Cl-II, closely matches the experimental spectrum and indicates that Cl-II is likely the most prevalent isomer found in experiment.

Calculated peaks at 1197 and 1317 cm^{-1} arise from N1-H1 in-plane bending in the presence of the chloride ion. In addition, there are carbonyl stretching and NH_2 scissoring modes calculated at 1734 and 1618 cm^{-1}, respectively. The calculated Cl-I spectrum is also a close match to the experimental spectrum. In this isomer, the O1 carbonyl stretch is apparent at 1728 cm^{-1}, along with the Cl---NH_2 scissoring at 1647 cm^{-1}. The experimentally observed peak at approximately 1450 cm^{-1} however, does not appear in the Cl-I spectrum. This peak arises from the interaction between chloride and H1 as observed in the Cl-II calculated spectrum. Nevertheless, based on the calculated energetics, it is probable that isomer Cl-I also exists to some extent under the experimental conditions.

The calculated harmonic, anharmonic and experimental spectra are shown in comparison in Figure 5.9. Calculated harmonic peaks from the in-plane bending of N1-H1 in the presence of the chloride ion located at 1197 and 1317 cm^{-1} have shifted to 1059 and 1277 cm^{-1}, respectively, and the carbonyl stretching and NH_2 scissoring modes at 1734 and 1618 cm^{-1} have shifted to 1707 and 1574 cm^{-1}, respectively, in the anharmonic spectrum. The vibrational modes at higher photon energies appear to be better approximated by the anharmonic calculation, whereas the vibrational modes at lower photon energy may be more harmonic in nature. Nevertheless, the calculated anharmonic spectrum is visibly red-shifted from the harmonic spectrum and thus, for many vibrational modes, allows for a better approximation of the experimental spectrum.[112-115]

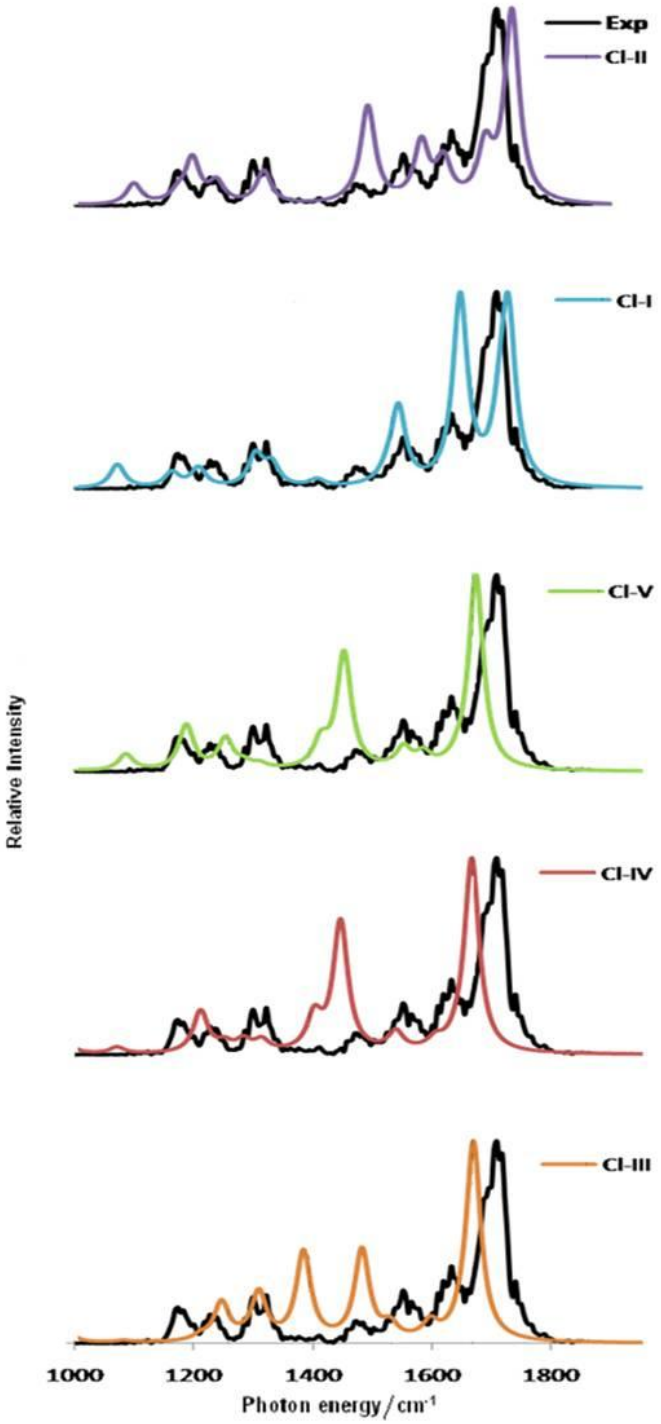

Figure 5.7: A comparison of the experimental spectrum with the harmonic calculated spectra for several isomers of the chloride-5-FC cluster. Harmonic spectra were calculated at the B3LYP/6-311+G(d,p) level of theory with a scaling factor of 0.9679.

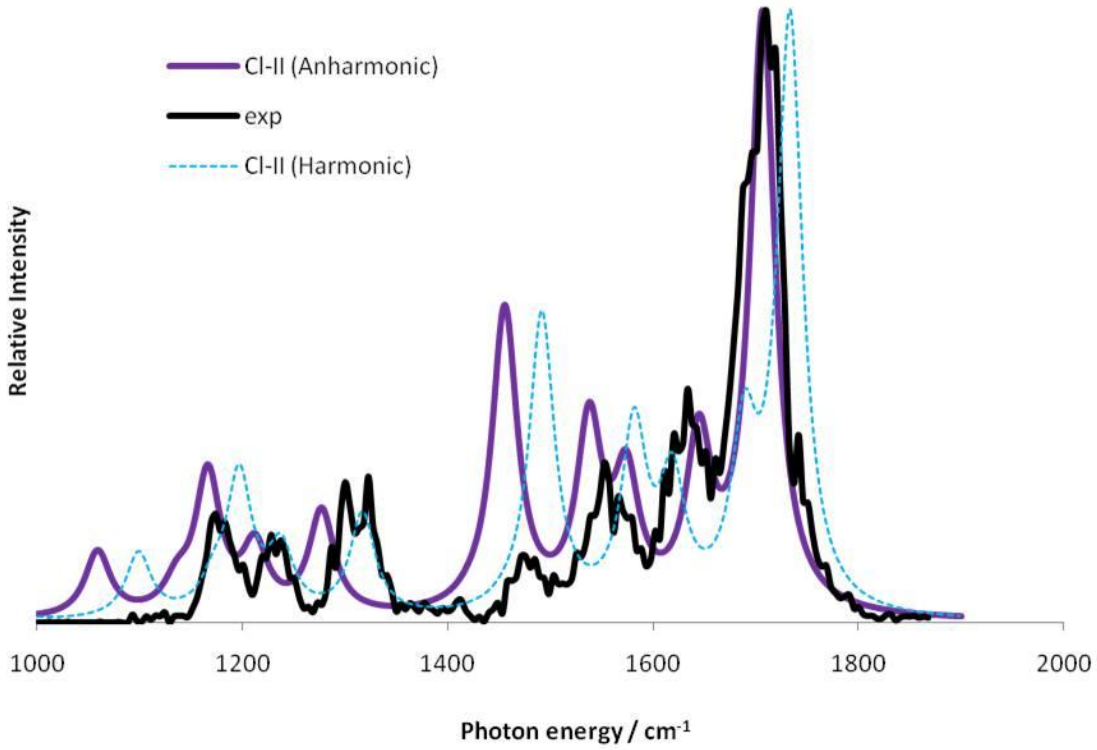

Figure 5.8: Calculated harmonic and anharmonic spectra in comparison with the experimental spectrum for Cl-II, the lowest energy isomer. Harmonic and anharmonic spectra were calculated at the B3LYP/6-311+G(d,p) level of theory, and harmonic frequencies were scaled by a factor of 0.9679.

5.3.4 5-Fluorocytosine Anionic Dimer

The IRMPD spectrum of the anionic dimer formed between deprotonated and neutral 5-FC has been obtained. Therefore, in order to begin geometry optimization calculations on this species, relevant deprotonated 5-FC isomers had to first be determined. Deprotonated isomers of 5-FC were optimized at the B3LYP/6-311+G(d,p) level of theory in order to obtain the energetically relevant deprotonated 5-FC isomers. By comparison of the relative

Gibbs free energies (298 K) of the deprotonated species, one energetically relevant deprotonated isomer was obtained; however, both FC-DP01 and FC-DP02 (Figure 5.10) were considered for the anionic dimers of 5-FC.

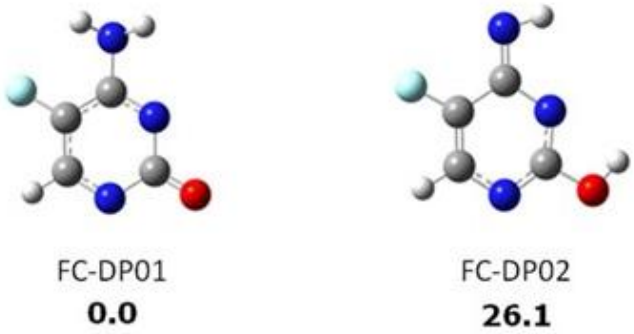

Figure 5.9: The two lowest energy calculated isomers of deprotonated 5-fluorocytosine. Relative Gibbs free energies (298 K) are reported in kJ/mol.

Over thirty-five combinations of deprotonated and neutral species were submitted for geometry optimizations. Combinations included FC-DP01 or FC-DP02 in association with a neutral (01, 03, or 04) in both planar and non-planar spatial conformations. Relative Gibbs free energies (298 K) of the calculated isomers for the 5-FC anionic dimers are shown in Figure 5.11 with the data indicating that a mixture of isomers is likely to be observed in experiment. The large number of energetically relevant isomers for the anionic dimer is not surprising due to the extensive number of possible combinations of deprotonated and neutral isomers.

Anionic-I

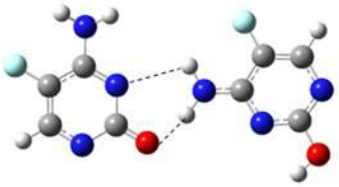

12.6

Anionic-II

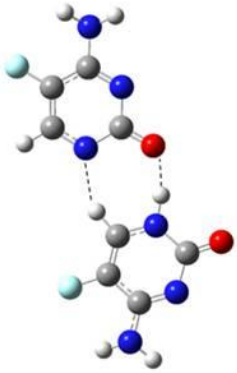

0.0

Anionic-III

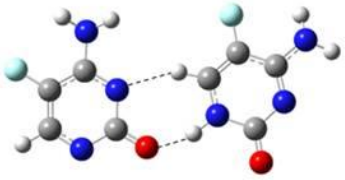

2.2

Anionic-IV

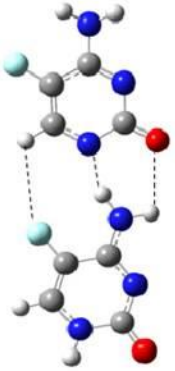

11.3

Anionic-V

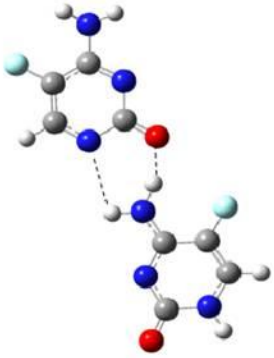

8.8

Anionic-VI

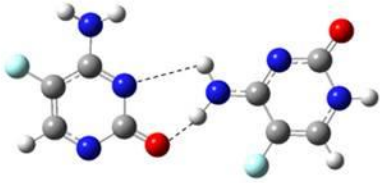

11.0

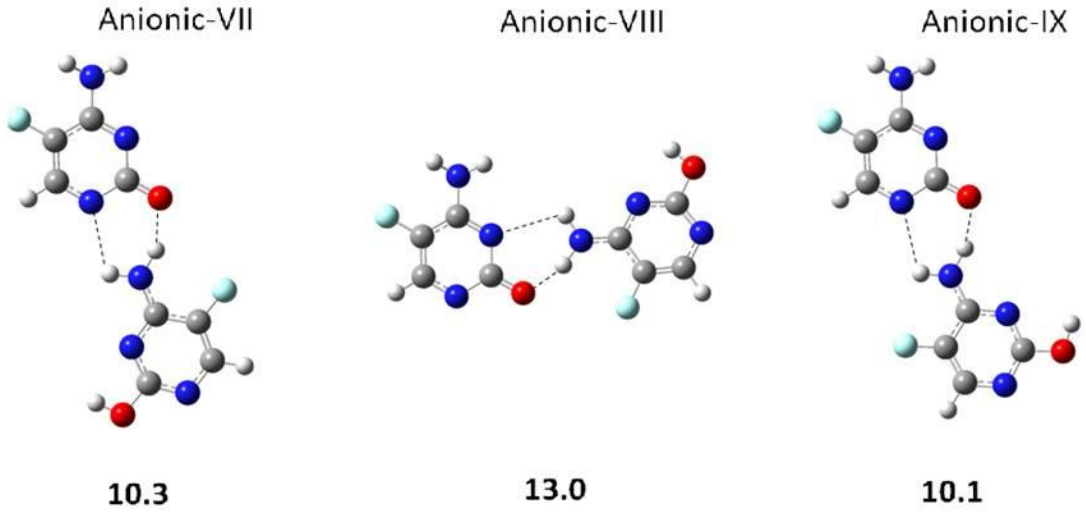

Figure 5.10: The nine energetically relevant 5-FC anionic dimers are shown with their relative Gibbs free energies (298 K) in kJ/mol. Ionic hydrogen bonds are indicated by dotted lines.

The calculated thermochemical data (298 K) of formation for several 5-FC anionic dimers is shown in Table 5.3. Values are based on formation as follows:

$$5\text{-FC}^- + 5\text{-FC} \rightarrow [5\text{-FC-5-FC}]^- \qquad \textbf{[5.3]}$$

Table 5.3: Thermochemical values (298 K) for formation of several isomers of the 5-fluorocytosine anionic dimer. Values have been calculated at the B2PLYP/aug-cc-pVTZ//B3LYP/6-311+G(d,p) level of theory. ΔH° and ΔG° values are reported in kJ/mol, ΔS° values are reported in J/ mol K.

Anionic Isomer	ΔH°	ΔS°	ΔG°
I	-95.3	-134	-55.5
II	-110	-148	-65.7
III	-106	-142	-63.7
IV	-94.2	-129	-55.7
V	-99.2	-134	-59.4
VI	-98.0	-137	-57.3
VII	-97.0	-132	-57.6
VIII	-95.0	-133	-55.4
IX	-97.2	-133	-57.7

The lowest energy calculated isomer is Anionic-II; however, eight other isomers have relative Gibbs free energies (298 K) within 15 kJ/mol of Anionic-II. All nine of the energetically relevant isomers involve bidentate interactions between the carbonyl oxygen of FC-DP01 and either FC-Neutral 01 or 04. The infrared spectra of the five lowest energy isomers are shown in Figure 5.12. For clarity, the 5-FC anionic dimers are labeled with the deprotonated species as species "A" and the neutral as species "B". The experimental spectrum appears to contain several isomers due to the extensive number of peaks found in the spectrum, which can be expected due to the similarity in energies of the calculated isomers.

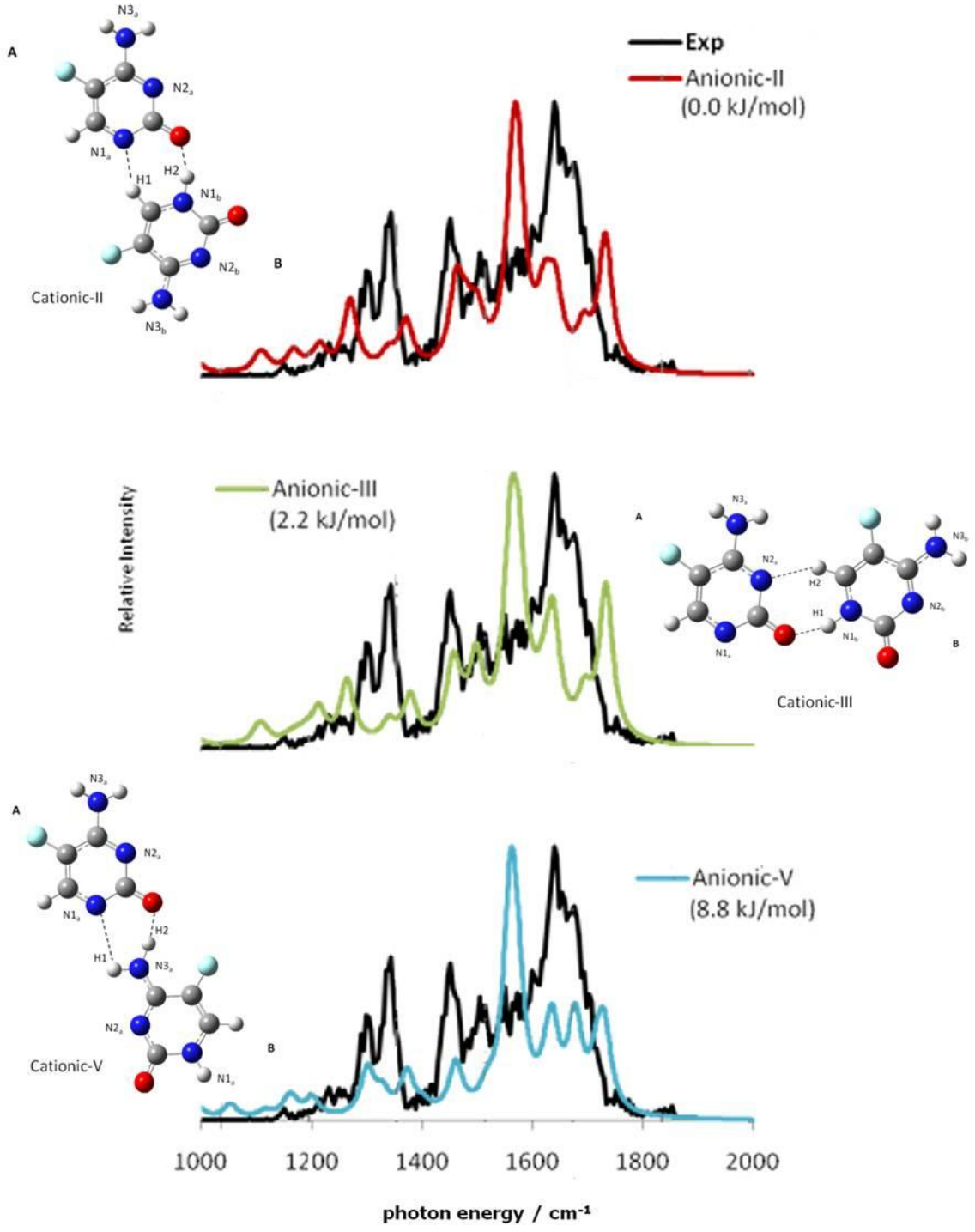
A
B
Exp
Anionic-II
(0.0 kJ/mol)
Cationic-II
Anionic-III
(2.2 kJ/mol)
Relative Intensity
Cationic-III
Anionic-V
(8.8 kJ/mol)
Cationic-V
1000
1200
1400
1600
1800
2000
photon energy / cm-1

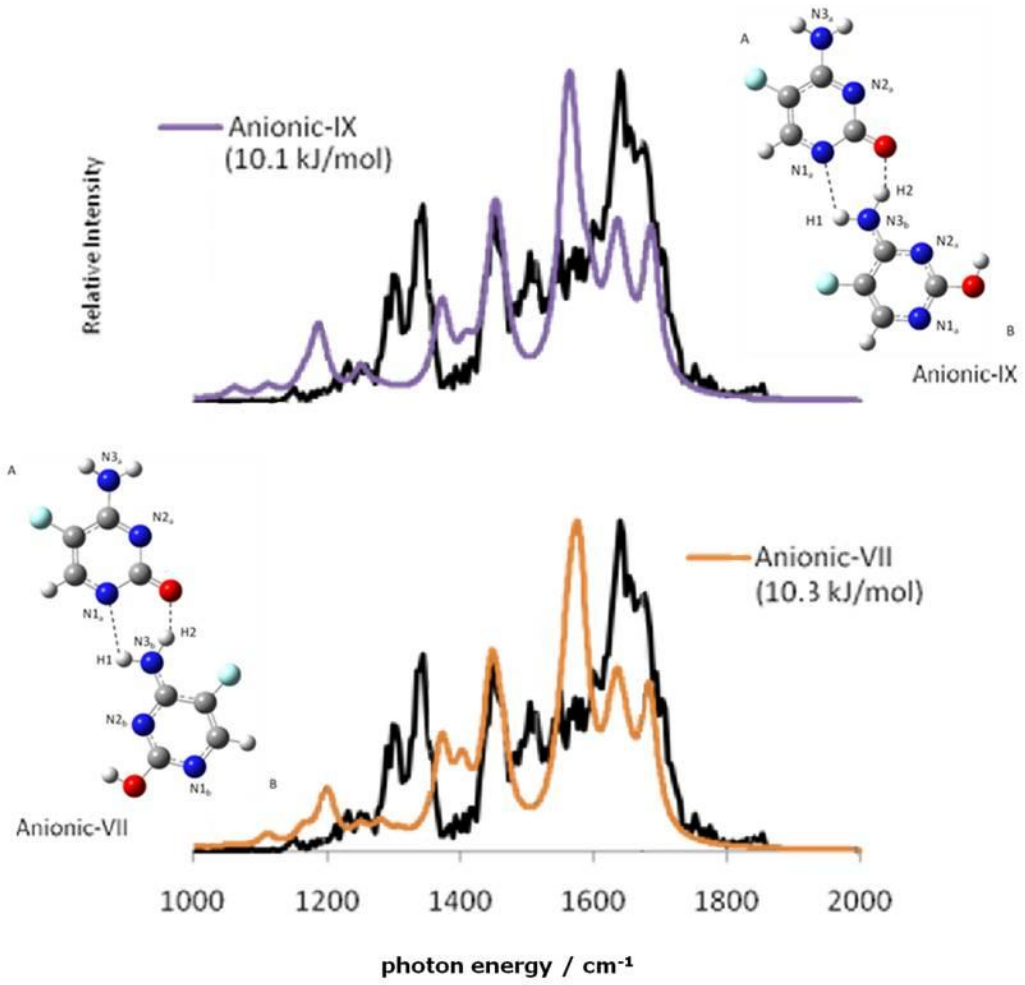

Figure 5.11: A comparison of the experimental and calculated harmonic spectra for the 5-fluorocytosine anionic dimer. The experimental spectrum is in black and the calculated spectra are in color. Harmonic spectra were calculated at the B3LYP/6-311+G(d,p) level of theory with frequencies scaled by a factor of 0.9679. Beside each spectrum, the corresponding 5-FC anionic dimer isomer is shown with hydrogen bonds indicated by dotted black lines. Relevant heteroatoms and hydrogens are labeled with numbers.

It is expected that a mixture of isomers is being observed in experiment. Based on the results of the harmonic calculations at the B3LYP/6-311+G(d,p) level of theory (scale of

0.9679), it is likely that spectral signatures of several isomers are contributing to the IRMPD spectrum of the anionic dimer of 5-FC. Peak assignments for the harmonic calculated spectra corresponding to Anionic-II, -III, and –V are listed in Tables 5.4, 5.5, and 5.6.

Table 5.4: Peak assignments for the anionic dimer of 5-fluorocytosine, Anionic-II.

Peak Location(s) (cm^{-1})	**Description**	**Atoms Involved**
1104, 1171, 1620	NH_2 in-plane bending	$N3_b$
1113, 1164, 1574	NH_2 in-plane bending	$N3_a$
1215, 1270, 1481	Asymmetric in-plane stretch of ionic hydrogen bonding protons	H1, H2
1574	Carbonyl stretch	$Carbonyl_a$
1732	Carbonyl stretch	$Carbonyl_b$
1692	Symmetric in-plane stretch of ionic hydrogen bonding protons	H1, H2

Table 5.5: Peak assignments for the anionic dimer of 5-fluorocytosine, Anionic-III.

Peak Location(s) (cm^{-1})	Description	Atoms Involved
1103, 1171, 1620	NH_2 in-plane bending	$N3_b$
1114, 1155, 1190, 1635	NH_2 in-plane bending	$N3_a$
1264	Asymmetric in-plane stretch of ionic hydrogen bonding protons	H1, H2
1339, 1498	Symmetric in-plane stretch of ionic hydrogen bonding protons	H1, H2
1561	Carbonyl stretch	$Carbonyl_a$
1733	Carbonyl stretch	$Carbonyl_b$

Table 5.6: Peak assignments for the anionic dimer of 5-fluorocytosine, Anionic-V.

Peak Location(s) (cm^{-1})	Description	Atoms Involved
1052	NH_2 in-plane bending	$N3_b$
1115, 1166	NH_2 in-plane bending	$N3_a$
1559, 1677	NH_2 scissoring	$N3_b$
1574	Carbonyl stretch	$Carbonyl_a$
1625	NH_2 scissoring	$N3_a$
1730	Carbonyl stretch	$Carbonyl_b$

It can be seen that the spectra do not vary greatly between each of the calculated isomers. This can be expected due to similarities in many of the low energy calculated

isomers. For example, the lowest energy isomer, Anionic-II involves an association between carbonyl$_a$ and N1$_a$ of FC-DP01 and H1 and H2 of FC-Neutral 01. The next lowest energy isomer, Anionic-III, is very similar but involves interaction with N2$_a$ instead of N1$_a$. This small change leads to a relative energy 2.2 kJ/mol higher than Anionic-II. Many of the calculated low energy isomers for the anionic dimer of 5-FC have only small differences, leading to small increases in their relative Gibbs free energies (298 K). The lowest energy interactions involve FC-DP01 and FC-Neutral 01, and calculations indicate that there are many ways in which these two species can interact within a small energy difference. Because of the great similarities in structure, energetics, and spectra of the calculated low energy isomers, it is likely that Anionic-II and Anionic-III are the most prevalent in experiment, among a mixture of some other calculated low energy isomers.

5.3.5 5-Fluorocytosine Cationic Dimer

The cationic dimer of 5-fluorocytosine has proven to be the most interesting of any of the 5-FC analogs studied. The cationic dimer is composed of one protonated species and one neutral species interacting through ionic hydrogen bonding interactions. Energetically relevant isomers of protonated 5-fluorocytosine have therefore been optimized in order to be considered for involvement in the cationic dimers. Each site of protonation on each of the neutral isomers of 5-FC has yielded only two isomers which will be considered experimentally accessible. All other calculated isomers for protonated 5-FC were in excess of 30 kJ/mol higher in relative Gibbs free energy (298 K). The two relevant protonated isomers are shown below in Figure 5.13.

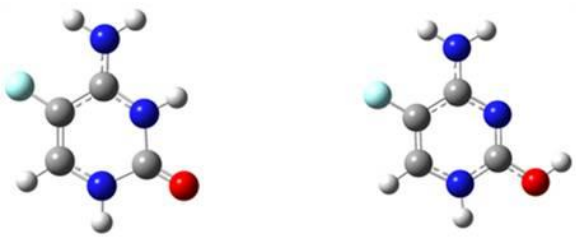

Figure 5.12: The energetically relevant protonated isomers of 5-fluorocytosine. Relative Gibbs free energies (298 K) are reported in kJ/mol.

Both FC-P01b and FC-P01c were considered for involvement in the cationic dimer of 5-FC, in combination with a relevant neutral isomer. Monodentate, bidentate, and tridentate interactions have been considered and optimized, in addition to both planar and non-planar complexes. Several calculated isomers are shown in Figure 5.14. The calculated Gibbs free energies (298 K) of these optimized structures strongly indicate Cationic-IV, a planar complex containing a tridentate interaction, will exist predominantly under the experimental conditions.

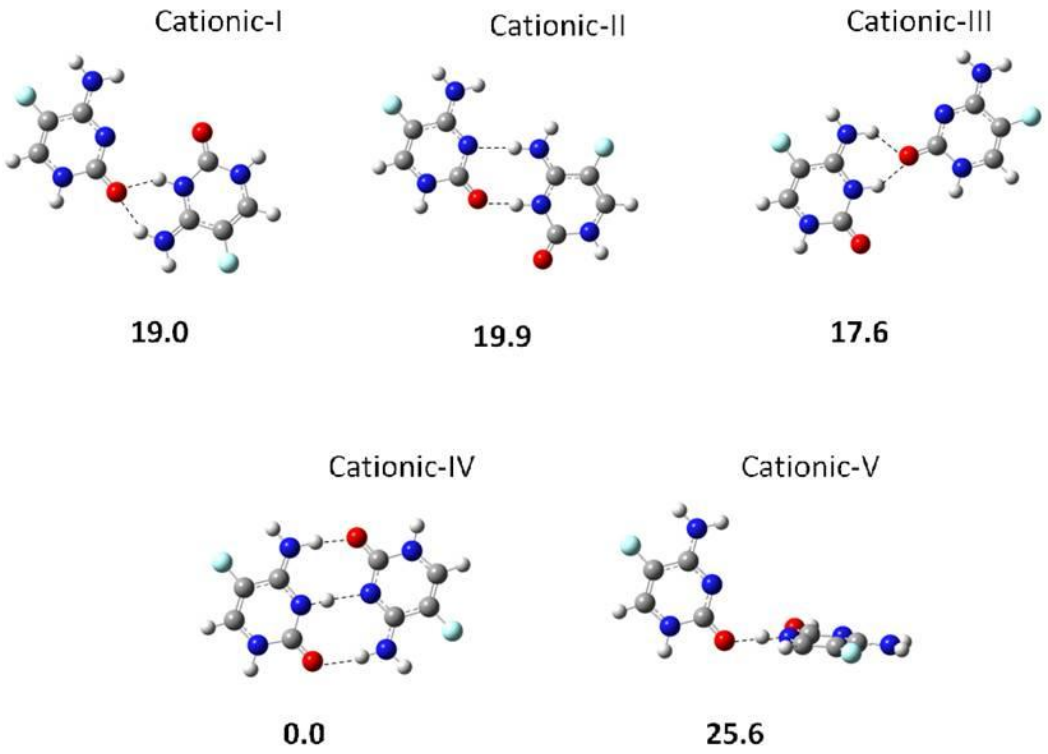

Figure 5.13: Structures of several isomers of the 5-fluorocytosine cationic dimer. Relative Gibbs free energies (298 K) are reported in units of kJ/mol

Calculated thermochemical values (298 K) for the formation of several cationic dimer isomers is shown in Table 5.7 below. Values are based on formation as follows:

$$5\text{-FCH}^+ + 5\text{-FC} \rightarrow [5\text{-FC-H-5-FC}]^+ \qquad \textbf{[5.4]}$$

Table 5.7: Thermochemical values (298 K) for the formation of several isomers of the 5-FC cationic dimer. Values have been calculated at the B2PLYP/aug-cc-pVTZ//B3LYP/6-311+G(d,p) level of theory and are reported in kJ/mol for ΔH° and ΔG° and in J/mol K for ΔS°.

Cationic Dimer	ΔH°	ΔS°	ΔG°
I	-154	-145	-78.1
II	-154	-158	-77.7
III	-141	-142	-66.0
IV	-187	-184	-99.7
V	-130	-140	-60.7

The tridentate ionic hydrogen bonding interaction found in this species is distinct due to the linear arrangement of all three ionic hydrogen bonds, leading to a very large calculated binding energy. Cationic-IV is shown in Figure 5.15 below with relevant heteroatoms labeled and hydrogen bonds represented by black dotted lines. Currently, the strongest known ionic hydrogen bond is found in $[F\text{-}HF]^-$, experimentally determined to be -192 (±6.7) kJ/mol.[116] The binding energy obtained for Cationic-IV is calculated to be 180 kJ/mol (B2PLYP/aug-cc-pVTZ//B3LYP/6-311+G(d,p)), suggesting that Cationic-IV may be a contender amongst some of the strongest ionic hydrogen bonds known. The magnitude of the calculated binding energy associated with this unique tridentate interaction convincingly suggests that the ionic hydrogen bonds involved in the formation of Cationic-IV are exceedingly strong!

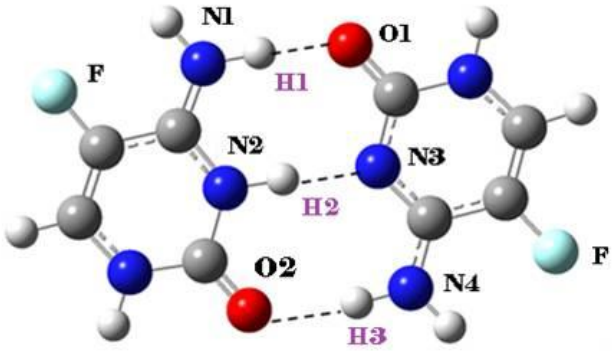

Figure 5.14: The lowest energy isomer, Cationic-IV, for the 5-FC cationic dimer. Heteroatoms and relevant hydrogens are labeled and hydrogen bonds are represented by black dotted lines.

Calculated bond lengths, relating to the three ionic hydrogen bonds of Cationic-IV, are shown in Table 5.8. The H1 ionic hydrogen bond between N1 and O1 has the shortest distance from heteroatom to heteroatom, suggesting that it is the strongest of the three ionic hydrogen bonds. In comparison, the H2 and H3 ionic hydrogen bonds grow subsequently farther apart by 0.12 Å and 0.28 Å, respectively.

Table 5.8: Theoretical bond lengths involved in the tridentate ionic hydrogen bond interaction of the cationic dimer isomer, Cationic-IV. Values are reported in Angstroms (Å).

Atoms Involved	Bond Length
Hydrogen bond of H1	
N1 to O1	2.70
N1 to H1	1.05
H1 to O1	1.66
Hydrogen bond of H2	
N2 to N3	2.82
N2 to H2	1.06
H2 to N3	1.75
Hydrogen bond of H3	
O2 to N4	2.98
O2 to H3	1.97
H3 to N4	1.02

Experimental and calculated vibrational spectra for several isomers of the 5-FC cationic dimer are shown in Figure 5.16. Many of the isomers are very similar in structure, simply varying by the site, orientation, or number of ionic hydrogen bonding interactions taking place. Each of the five lowest energy isomers shown in Figure 5.12 involves FC-Neutral 01 interacting with either FC-P01b or FC-P01c. Cationic-I, -II and –IV each have FC-Neutral 01 interacting with FC-P01b. Cationic-V involves an association between FC-Neutral 01 and FC-P01c, is a non-planar isomer, and is higher in energy than the other four

isomers. Therefore, due to the great similarity in structure between the calculated isomers for the 5-FC cationic dimer, the calculated spectra do not unambiguously assign a dominant isomer for this species. The relative Gibbs free energies (298 K) of these species however, do strongly indicate that Cationic-IV is the likely species observed in experiment. Cationic-III has a relative Gibbs free energy (298 K) of 17.6 kJ/mol and is the next lowest energy isomer in comparison to Cationic-IV. Although several isomers may be present under the experimental conditions, Cationic-IV should be the most abundant. The peak assignments corresponding to the calculated Cationic-IV spectrum are shown in Table 5.9.

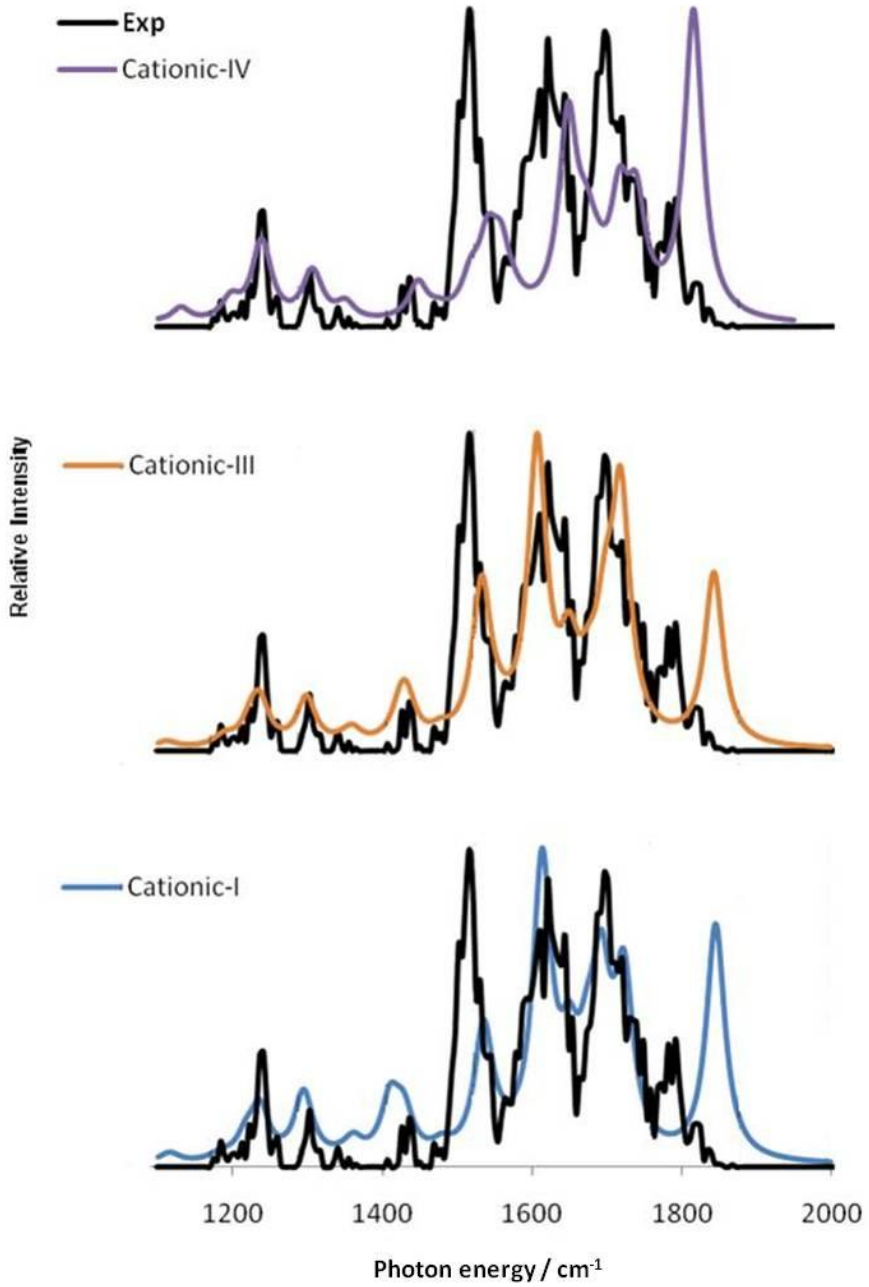

Figure 5.15: The experimental spectrum for the 5-FC cationic dimer in comparison with harmonic calculated spectra from several isomers. The experimental spectrum is represented in black and the calculated spectra are in color. Harmonic spectra were calculated at the B3LYP/6-311+G(d,p) level of theory with frequencies scaled by a factor of 0.9679.

Table 5.9: Vibrational spectrum peak assignments for the 5-fluorocytosine cationic dimer isomer, Cationic-IV.

Peak Location(s) (cm^{-1})	Description	Atoms Involved
1237. 1517, 1647	NH_2 in-plane rocking	N1
1558, 1576,1647, 1671, 1716, 1738, 1815	Orthogonal proton motion between N2 and N3	H2
1303, 1540, 1671, 1716	NH_2 in-plane rocking	N4
1738	Symmetric carbonyl stretch	O1, O2
1815	Carbonyl stretch	O2

5.4 Conclusions

IRMPD spectroscopy in combination with electronic structure calculations has again been shown to be a valuable tool for structural elucidation. For each of the 5-fluorocytosine analogs considered, a single predominant species has been proposed, except for the anionic dimer, in which a mixture of isomers is determined to be most probable. The B3LYP/6-311+G(d,p) level of theory used for all geometry optimizations has provided calculated spectra which approximate the experimental spectra exceptionally well, and thus has also facilitated the characterization of each species of interest. Single point calculations at the B2PLYP/aug-cc-pVTZ level of theory were used to more accurately approximate the electronic energies of each of the systems investigated and thus, should provide more accurate thermochemical values.

Trimethylammonium is observed to associate with 5-fluorocytosine at the carbonyl oxygen of 5-FC, as observed in isomer TMA-I. The proton involved in the ionic hydrogen bond interaction of this cluster has been calculated to reside closer to the nitrogen of trimethylamine rather than the oxygen atom of 5-FC. The calculated spectrum for TMA-I has significant peaks at 1621 and 1660 cm^{-1}, corresponding to the carbonyl stretch in asymmetric motion with the proton of trimethylammonium. Calculated spectra of other trimethylammonium-5-FC clusters yield peaks which are shifted from the experimental spectrum, due to their ionic hydrogen bonding interactions occurring at alternate sites. Overall, the calculated spectra of TMA-I matches the experimental spectrum remarkably well.

For the cluster involving chloride in association with 5-FC, a set of potentially relevant isomers has been calculated based on their relative energetics. The calculated spectrum for the lowest energy isomer, Cl-II, qualitatively matches the experimental spectrum more so than the calculated spectra from the other isomers. The peak around 1710 cm^{-1} in the experimental spectrum appears to be from the carbonyl stretch and is found only in the calculated spectra of Cl-II and Cl-I, since in the other isomers, the oxygen is not in keto form. Because of their equally close match in calculated spectra, isomers Cl-II and Cl-I are likely both present in experiment; however, based on their relative energetics, Cl-II is likely to be the most abundant.

In experiment, the anionic dimer of 5-fluorocytosine likely exists as a mixture of several isomers. Over thirty 5-FC anionic dimer isomers were optimized and nine were determined to be energetically relevant. All nine of the energetically relevant isomers

involve bidentate interactions between the carbonyl oxygen of FC-DP01 and a nitrogen atom on either FC-Neutral 01 or FC-Neutral 04. A mixture of isomers appears to be present in the experimental spectrum due to the substantial number of spectral signatures observed that cannot be attributed to a single dominant isomer.

The cationic dimer of 5-FC is found to likely exist as a single dominant species with a very interesting tridentate ionic hydrogen bonding interaction. The three ionic hydrogen bonds formed in this dimer are very efficient and result in an exceptionally large calculated binding energy (B2PLYP/aug-cc-pVTZ//B3LYP/6-311+G(d,p)), with a value of 180 kJ/mol. Due to the similarity in structure of many of the lower energy calculated isomers, the spectra for these species do not irrefutably identify the species being observed in experiment; however, the relative Gibbs free energies (298 K) of the 5-FC cationic dimers do indicate that Cationic-IV, which contains the tridentate ionic hydrogen bonding interaction, should be the dominant isomer in experiment.

Chapter 6
A Parallel and Sequential Fragmentation Mechanism of Protonated Ferulic Acid by IRMPD Spectroscopy and Electronic Structure Calculations

6.1 Introduction

Ferulic acid is a derivative of phenylalanine and cinnamic acid found in the cell walls of plants. Due to its conjugation and rigidity, it is a vital structural component and gives strength to the cell wall of many plant species.[117-119] The presence of ferulic acid has also been associated with defense mechanisms against viruses, insects, and pathogens, in addition to protection against enzymatic hydrolysis.[119] The concentration of ferulic acid in plant cells can have an effect on the speed of decay relating to plant organic matter in the soil, due to ferulic acid's inhibition of plant pathogens.[120]

In addition to ferulic acid being a vital component in the tissues of many plants, it is widely used in therapeutic products due to its strong UV absorption abilities and for its antioxidant properties.[121-124] Ferulic acid has been employed in the use of therapeutics relating to cancer, diabetes, and aging as well as cardiovascular and neurodegenerative disease.[124] The UV absorption abilities of ferulic acid are due to its effective reactivity with free radicals. Reactive oxygen species (ROS) such as the superoxide anion, hydroxyl radical, and hydrogen peroxide can be scavenged and prevented by ferulic acid's antioxidant action.[124]

Ferulic acid is commercially used as a bitterness inhibitor in order to mask the bitterness of several artificial sweeteners such as saccharin and acesulfame K.[125] The addition of ferulic acid to consumable materials also inhibits lipid peroxidation and consequent spoiling due to oxidation.[122, 124] It is typically desirable to use natural rather than synthetic antioxidants in foods, and ferulic acid and its derivatives are considered to be some of the most important antioxidants obtained from oats.[126]

6.2 Methods

IRMPD spectroscopy experiments were performed as described in Chapter 2. Solutions of protonated ferulic acid with a concentration of approximately 10^{-6} M were prepared by dissolving solid ferulic acid in a 1:1 mixture of acetonitrile and water, and a small amount of formic acid.

All geometry optimization and frequency calculations were performed at the B3LYP/6-311+G(d,p) level of theory, with the harmonic frequencies scaled by a factor of 0.9679.[71, 86, 109-110] Anharmonic frequencies have been calculated at the same level of theory for the lowest energy isomers Fer1b and Fer2a, corresponding to ions of m/z 195 and 177, respectively.

6.3 IRMPD of Protonated Ferulic Acid

Due to its extensively conjugated structure, IRMPD experiments involving protonated ferulic acid resulted in a very unique and interesting fragmentation mechanism, since several stable

fragment ions can be formed. Following IRMPD, protonated ferulic acid (m/z 195) gives rise to three fragment ions that can be observed simultaneously (m/z 177, 163, and 149). Fragmentation mechanisms for the IRMPD of protonated ferulic acid have been proposed and will follow.

6.4 Neutral Ferulic Acid

Calculated isomers of neutral ferulic acid are shown below in Figure 6.1. FA-Neutrals 01 and 03 have been calculated to be energetically favourable, likely because the hydrogen attached to the OH group of the acid is directed away from the side chain sp^2 hydrogen atoms, reducing steric hindrance.

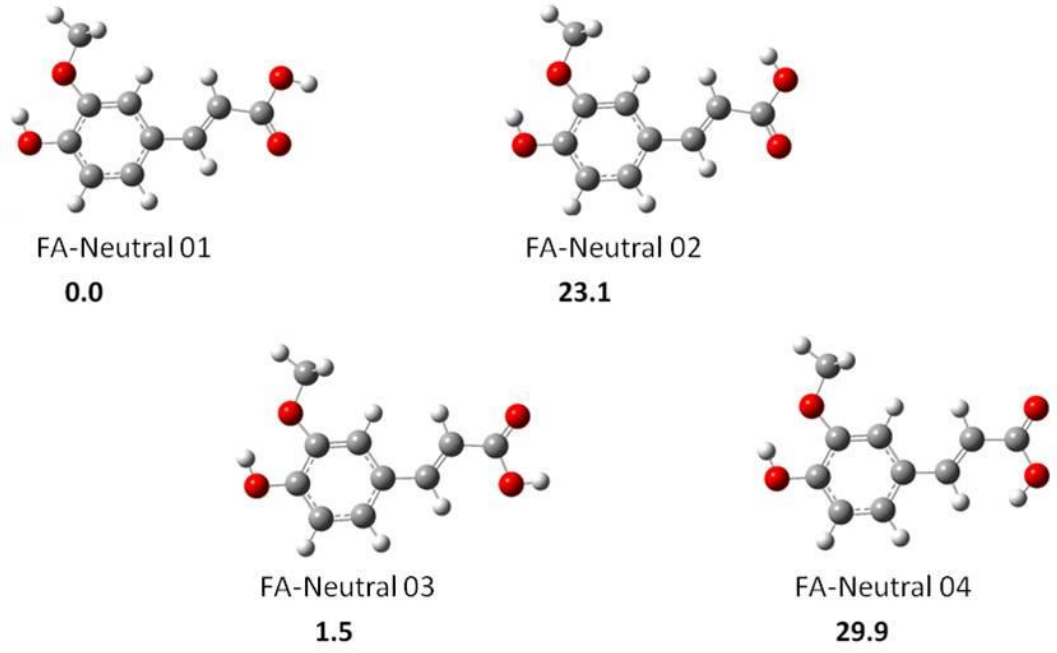

Figure 6.1: The calculated neutral isomers of ferulic acid with relative Gibbs Free energies (298 K) shown in kJ/mol.

Since protonated ferulic acid is being observed in the IRMPD experiments, it is important to first consider the site of protonation on neutral ferulic acid. Electronic structure calculations in combination with the IRMPD spectrum of protonated ferulic acid have been used in order to determine if protonation occurs at the carbonyl or hydroxyl oxygens of the acid functional group, the methoxy group, or the phenolic group. Several isomers were calculated for each site of protonation and a lowest energy isomer was found for each, shown below in Figure 6.2.

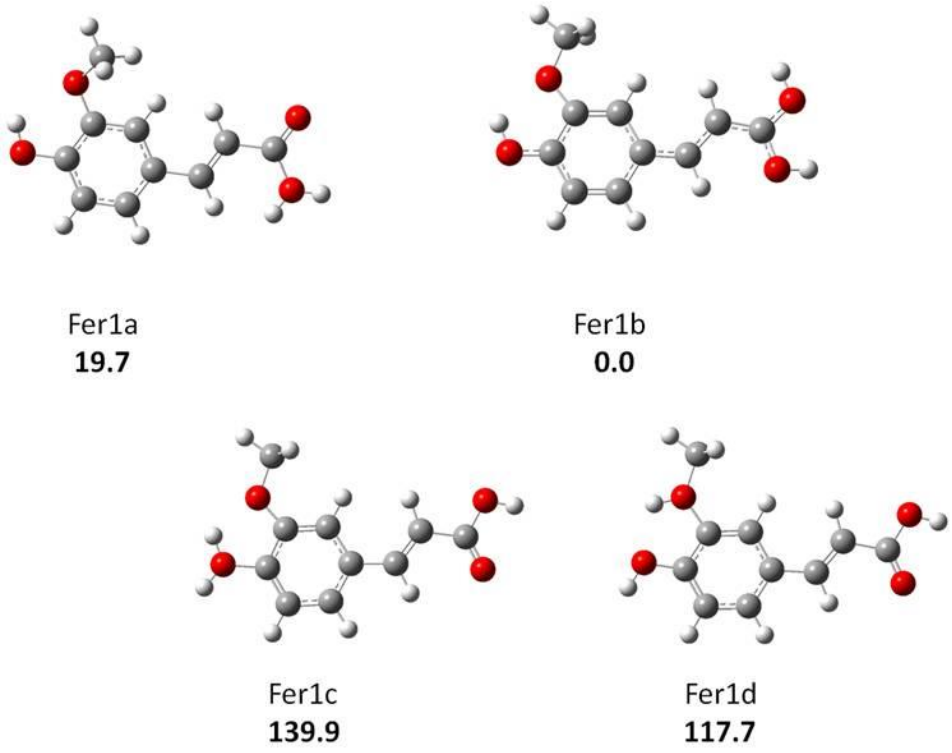

Figure 6.2: The lowest energy calculated isomers for each potential site of protonation on ferulic acid. Relative Gibbs free energies (298 K) are shown in kJ/mol.

Proton affinities and gas basicities have been calculated for each potential site of protonation and are shown in Table 6.1. The carbonyl at site B has the highest calculated proton affinity.

Table 6.1: The calculated proton affinities and gas basicities (298 K) of several relevant sites on neutral ferulic acid in kJ/mol. Heteroatom sites are labeled on the neutral structure to the left.

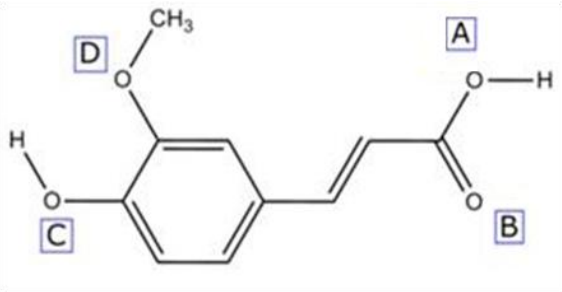

Heteroatom Site	Proton Affinity	Gas Basicity
A	860	843
B	896	863
C	746	723
D	774	745

The IRMPD spectrum of protonated ferulic acid (m/z 195) strongly suggests that the initial site of protonation is at the carbonyl oxygen of the acid functional group. The lowest energy isomer for each site has been compared with the IRMPD spectrum of protonated ferulic acid (Figure 6.3). Isomer Fer1b, corresponding to protonation at site B on the carbonyl oxygen of the acid has been determined to best match the experimental spectrum. The harmonic calculated spectra corresponding to isomers Fer1d, Fer1a, and Fer1c each have significant peaks which are characteristic of their conformation, but differ from the experimental spectrum. The calculated spectrum of Fer1d has such a peak at 1421 cm^{-1} which results from the proton rocking on the methoxy group. In addition to this, there is the beginning of a large peak at 1801 cm^{-1} that corresponds to carbonyl stretching motion. This peak is not seen in the experimental spectrum, further indicating that the carbonyl oxygen is

the site of protonation. For isomer Fer1a, the large peak at 1150 cm^{-1} in the experimental spectrum is not accounted for. This missing peak corresponds to rocking of the alcohol in the COOH group, which in isomer Fer1a has been protonated to form water. Because protonation at this site forms water which likely dissociates instantly, a carbonyl peak is not seen in this species. The calculated spectrum of Fer1c however, does have a carbonyl peak at 1800 cm^{-1}, since this species does not involve protonation of the hydroxyl or carbonyl oxygen atoms, but protonation of the phenolic oxygen. The spectrum of Fer1c also has peaks at 1027 and 1535 cm^{-1} resulting from the symmetric and asymmetric rocking of the R-$^{+}OH_2$ hydrogens, respectively. Another peak calculated to occur at 1080 cm^{-1}, arises from the R-$^{+}OH_2$ stretch; however, this signature is not observed in the IRMPD spectrum. Therefore, because of these differences, the calculated spectrum of Fer1b matches the experimental spectrum most closely. Peak assignments for Fer1b are shown in Table 6.2.

Table 6.2: Peak assignments for isomer Fer1b of m/z 195.

Peak (cm^{-1})		
Harmonic	**Anharmonic**	**Description**
1167, 1199	1130, 1149	$COOH_2^{+}$ rocking
1369	1339	Phenolic stretch
1509	1474	Methoxy scissoring
1610	1572	Rocking of the phenolic and acid OH groups

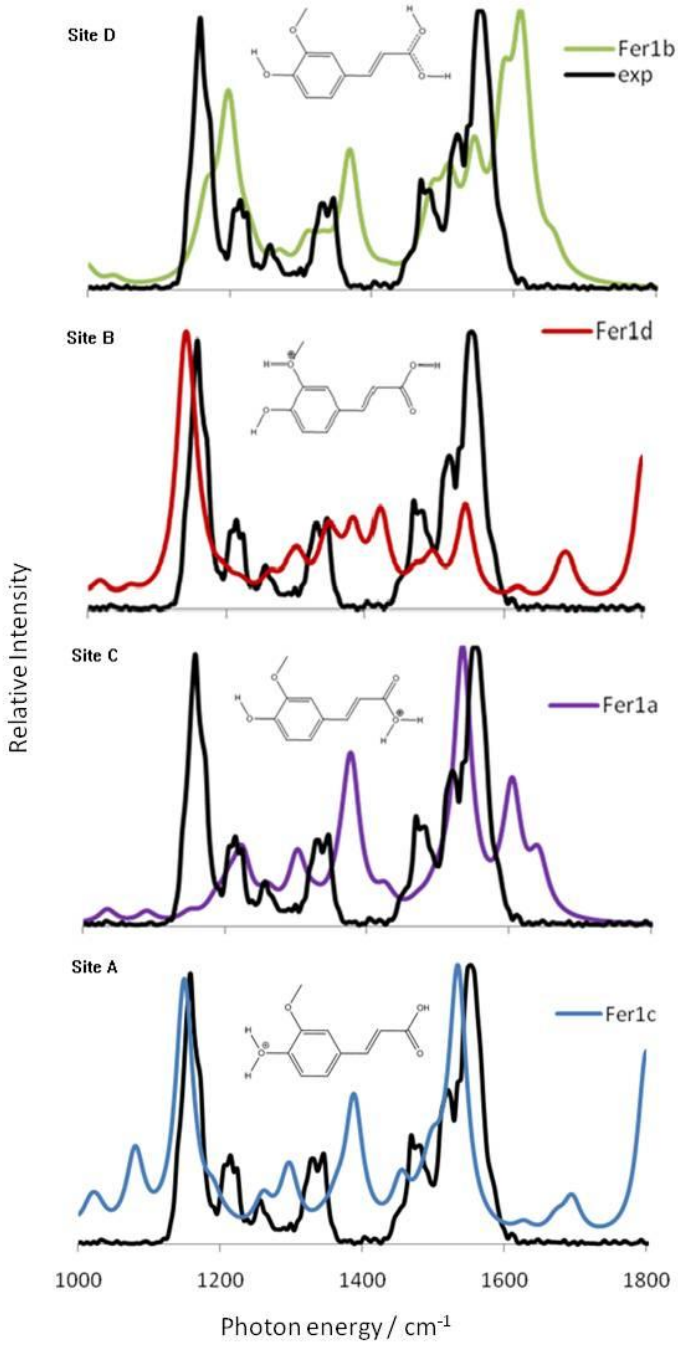

Figure 6.3: A comparison of the experimental and harmonic calculated spectra for protonated ferulic acid (m/z 195). The experimental spectrum is represented in black and the calculated spectra are in color. Harmonic spectra were calculated at the B3LYP/6-311+G(d,p) level of theory with frequencies scaled by 0.9679.

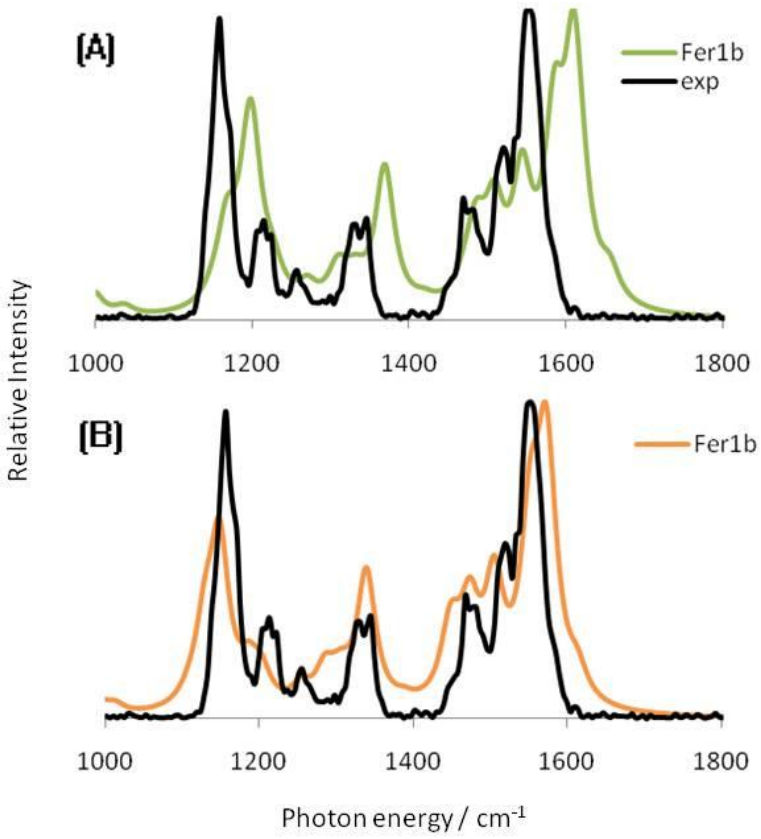

Figure 6.4: The experimental m/z 195 spectrum in comparison with the calculated (A) harmonic and (B) anharmonic spectra for isomer Fer1b. Harmonic and anharmonic spectra were calculated at the B3LYP/6-311+G(d,p) level of theory, harmonic frequencies were scaled by a factor of 0.9679.

Both the harmonic and anharmonic calculated spectra for isomer Fer1b are found to best match the experimental spectrum (Figure 6.4). Characteristic peaks resulting from asymmetric rocking of the two hydroxyl groups in the $COOH_2^+$ functionality are located at 1199, 1149, and 1157 cm^{-1}, for the calculated harmonic, anharmonic, and experimental spectra, respectively. The calculated anharmonic spectrum matches the experimental spectrum very closely, further suggesting that the carbonyl protonated species is being observed in experiment.

In addition to spectral comparisons, isomer Fer1b has been calculated to be the lowest energy isomer for protonated ferulic acid based on the relative Gibbs free energies (298 K) calculated for a number of isomers for each potential site of protonation, as shown in Figure 6.2. Based on the calculated Gibbs free energies (298 K) of additional calculated isomers, it is found that ferulic acid is consistently lowest in energy when all of the atoms lie in a single plane. Table 6.3 contains the relative thermochemical values (298 K) of the lowest energy isomer for each potential site of protonation on ferulic acid. Isomer Fer1b, corresponding to protonation on the carbonyl oxygen, has been calculated to be approximately 20 kJ/mol lower in Gibbs free energy (298 K) than the hydroxyl protonated species, which is the next lowest energy structure found. Therefore, based on both spectra and energetics, it is expected that neutral ferulic acid is protonated on the carbonyl oxygen.

Table 6.3: Calculated relative energetics for the lowest energy m/z 195 isomers corresponding to each site of protonation. Values were calculated at the B3LYP/6-311+G(d,p) level of theory and are reported in kJ/mol for $\Delta G_{rel}°$ and $\Delta H_{rel}°$ and in J/mol K for $\Delta S_{rel}°$.

Isomer	Site of Protonation	$\Delta H_{rel}°$	$\Delta S_{rel}°$	$\Delta G_{rel}°$
Fer1a	A	35.3	-52.6	19.7
Fer1b	B	0.0	0.0	0.0
Fer1c	C	149.6	-32.7	139.9
Fer1d	D	122.0	-14.5	117.7

Protonation on the carbonyl oxygen has been calculated to be most favourable; however, in addition to isomer Fer1b, there are two other energetically relevant isomers

corresponding to protonation at this site, shown in Figure 6.5 below. Based on the relative Gibbs free energies (298 K) of the isomers, Fer1b is likely the most abundant isomer of protonated ferulic acid; however, the other isomers shown may also be present to some extent.

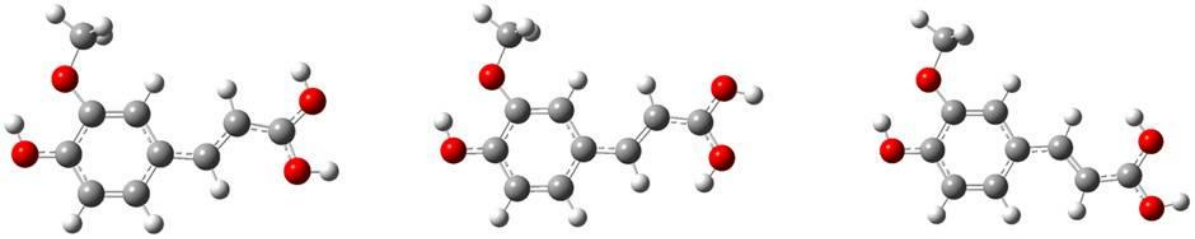

Figure 6.5: The energetically relevant isomers of protonated ferulic acid. Relative Gibbs free energies (298 K) are shown in kJ/mol.

6.5 Proposed Mechanism

Two parallel fragmentation mechanisms are proposed for the formation of the three fragment ions (m/z 177, 163, and 149) observed during the IRMPD of protonated ferulic acid. Scheme 1 (Figure 6.6) shows the formation of m/z 177 and 149 due to loss of water and carbon monoxide, respectively.

6.5.1 <u>Scheme 1</u> – The mechanism of formation for the ions of m/z 177 and 149

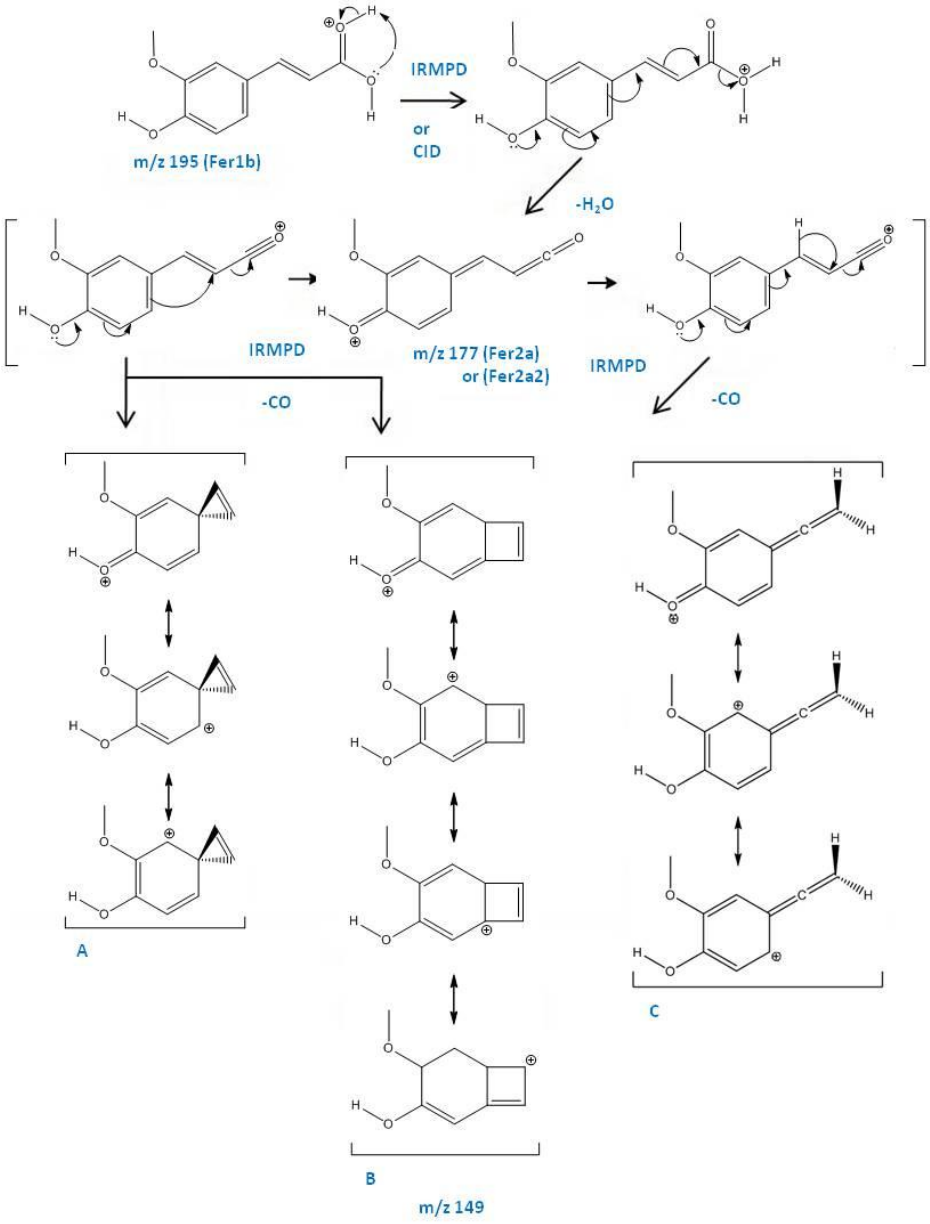

Figure 6.6: Scheme 1 of the proposed fragmentation mechanism for ferulic acid. IRMPD leads to proton transfer and loss of water, resulting in an ion of m/z 177. Subsequent IRMPD leads to loss of carbon monoxide, forming an ion of m/z 149.♦

♦ A special thanks to Dr. Rick Marta for his help with the proposed mechanisms.

Proton transfer occurs from the initial site of protonation on the carbonyl oxygen to the hydroxyl oxygen of the acid group. The endothermic loss of water (35.6 kJ/mol) leads to an ion of m/z 177 which can be considered to be a resonance hybrid between acylium ($-C\equiv O^+$) and ketene ($-C^+=C=O$) structural moieties. Several starting structures of the ion of m/z 177 were considered, however, all calculated isomers converged to two isomers, Fer2a and Fer2a2. Fer2a and Fer2a2 are shown below in Figure 6.7 with their relative Gibbs free energies in kJ/mol.

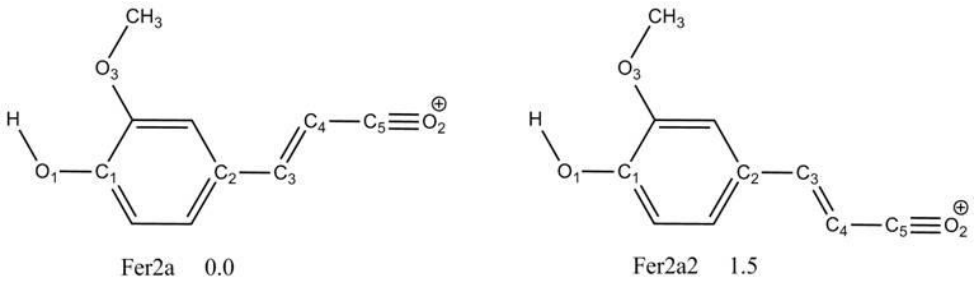

Figure 6.7: The calculated isomers of m/z 177 shown in acylium-type form. Relative Gibbs free energies (298 K) are shown in kJ/mol. Relevant atoms are labeled by number.

These two isomers are very similar; however, based on their relative Gibbs free energies (298 K) differing by only 1.5 kJ/mol, both species will likely be present in experiment. Comparisons of the calculated and experimental spectra are shown in Figure 6.8. The harmonic calculated spectrum of isomer Fer2a has a peak at 1221 cm^{-1} corresponding to rocking of the phenolic and methoxy groups. Stretching of the sp^2 carbons in the molecule gives rise to a peak at 1535 cm^{-1} and the large peak located at 2260 cm^{-1}

results from the stretching motion of the acylium moiety. These peaks are located, respectively, at 1192, 1494, and 2220 cm^{-1} in the calculated anharmonic spectrum. The anharmonic spectrum is found to be red shifted relative to the calculated harmonic spectrum and also, match the IRMPD spectrum more closely. This seems reasonable since the vibrational modes in this molecule are likely more anharmonic in nature due to protonated ferulic acid being a heavily conjugated molecule.

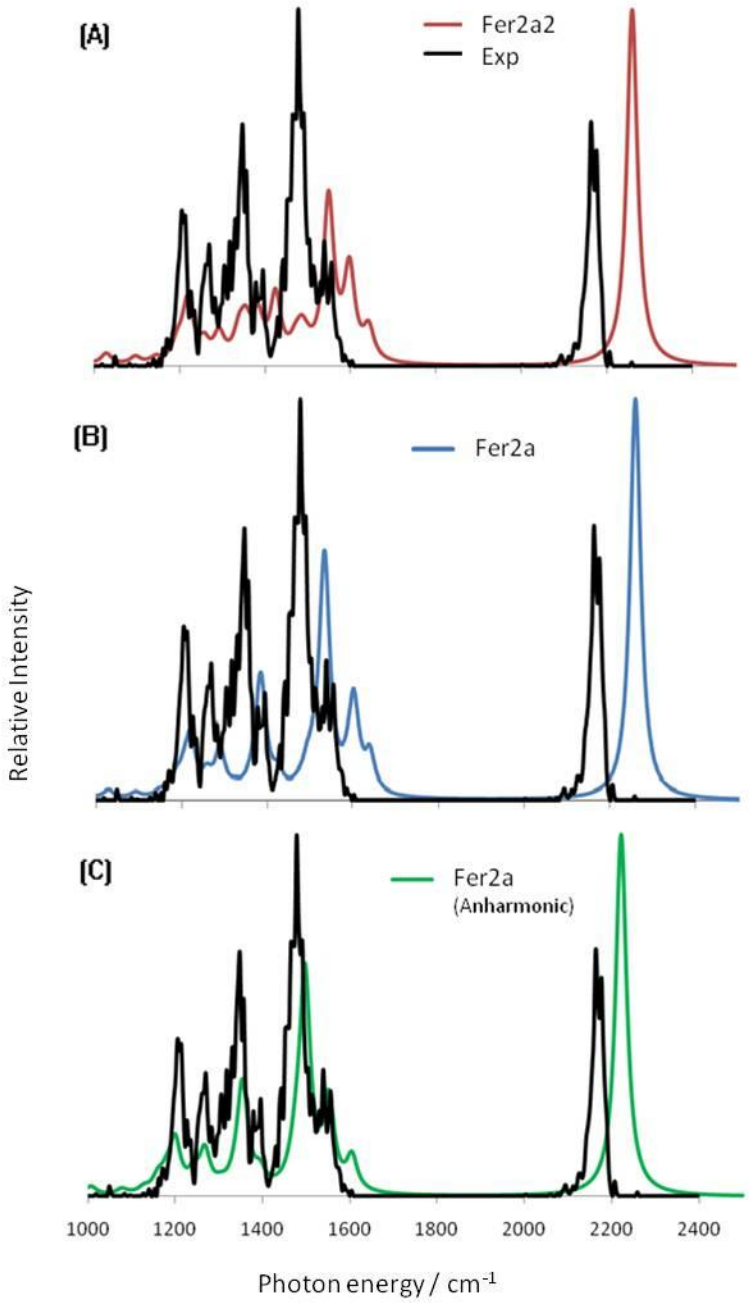

Figure 6.8: A comparison of the experimental m/z 177 spectrum with (A) the harmonic calculated Fer2a2 spectrum and (B) the harmonic calculated Fer2a spectrum. In (C), the calculated anharmonic Fer2a spectrum is shown in comparison with the experimental spectrum. Harmonic and anharmonic spectra were calculated at the B3LYP/6-311+G(d,p) level of theory and harmonic frequencies have been scaled by 0.9679.

Calculated bond lengths for the Fer2a isomer of m/z 177 are shown below in Table 6.4 and indicate that the acylium ion structure is most representative of the resonance hybrid. A carbon-carbon single bond (in the presence of an aromatic ring) and simple double bonds are typically around 1.53 and 1.34 Å, respectively.[9] Carbon-oxygen single, partial double, double, and partial triple bonds are typically around 1.43, 1.36, 1.26, and 1.20 Å, respectively.[9]

Table 6.4: The bonds and calculated bond lengths for the Fer2a isomer of m/z 177. Atoms are labeled in Figure 6.7 and bond lengths are shown in Angstroms (Å).

Atoms	Bond Length
O1 – C1	1.32
C2 – C3	1.40
C3 – C4	1.40
C4 – C5	1.35
C5 – O2	1.14
C8 – O3	1.35

Following IRMPD, ion m/z 177 subsequently loses carbon monoxide to form a fragment of m/z 149. In order to probe the structure and mechanism of formation of this product, m/z 177 was formed by collision induced dissociation (CID) and subsequently subjected to IRMPD. Presuming that the m/z 177 formed by CID is identical to that resulting from IRMPD, the subsequent loss of CO can be considered.[127-129] Three possible isomers for this ion have been successfully optimized and are shown in Figure 6.6; however, due to the

significant ring strain present in the three and four membered ring containing structures, the allene structure is favoured, and therefore, the most likely species to exist under the experimental conditions. An isomer containing an 8-membered ring was considered; however, upon optimization, the 8-membered ring collapsed to a 4-membered ring. The relative energetics of the three calculated m/z 149 isomers are shown in Table 6.5 below.

Table 6.5: Relative energetics for the three calculated m/z 149 isomers reported in kJ/mol for $\Delta H_{rel}°$ and $\Delta G_{rel}°$, and in J/mol K for $\Delta S_{rel}°$. Values have been calculated at the B3LYP/6-311+G(d,p) level of theory.

Isomer	**$\Delta H_{rel}°$**	**$\Delta S_{rel}°$**	**$\Delta G_{rel}°$**
Mz149-A (3-Membered)	105.8	-7.8	108.2
Mz149-B (4-Membered)	105.6	-14.5	109.9
Mz149-C (Allene)	0.0	0.0	0.0

Simple bond cleavage to lose CO thus gives rise to an allene-like structure for m/z 149. The structure and relevant bond lengths of the allene-like isomer for m/z 149 are shown in Table 6.6. Ideally, the structure of m/z 149 would also have been probed by IRMPD; however, there was insufficient intensity in this fragment to make it feasible.

Table 6.6 Structure and bond lengths for the allene-like isomer of m/z 149. Bond lengths are reported in Angstroms (Å).

Structure	Atoms	Bond Length
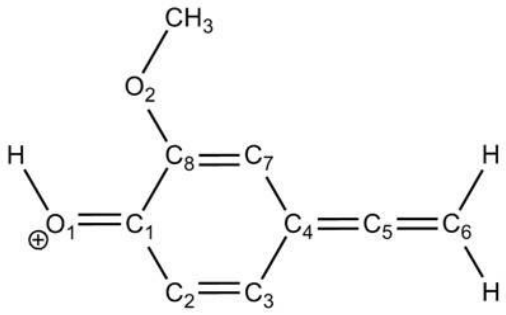	$O_1 – C_1$	1.31
	$C_1 – C_2$	1.41
	$C_2 – C_3$	1.37
	$C_3 – C_4$	1.44
	$C_4 – C_5$	1.35
	$C_5 – C_6$	1.29
	$C_4 – C_7$	1.44
	$C_7 – C_8$	1.37
	$C_8 – C_1$	1.44
	$C_8 – O_2$	1.35

6.5.2 Scheme 2 – The mechanism of formation for the ion of m/z 163

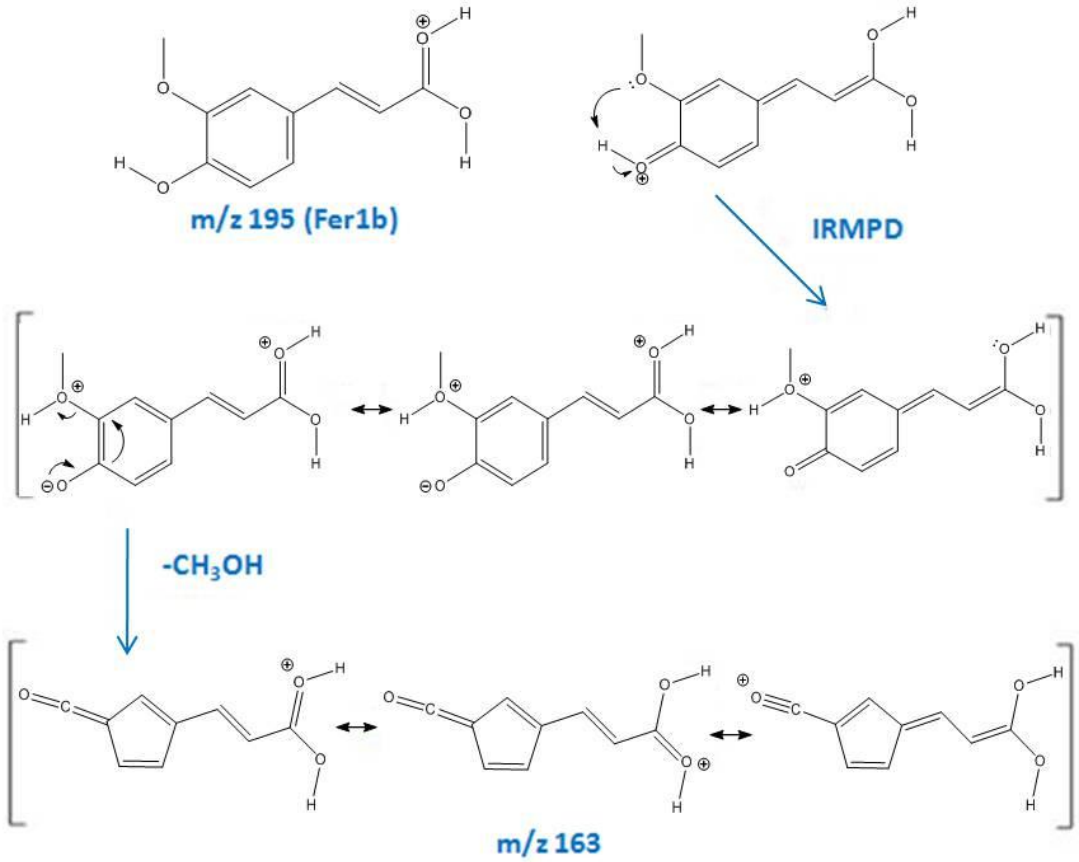

Figure 6.9: Scheme 2 of the proposed fragmentation mechanism for ferulic acid. IRMPD leads to proton transfer and loss of methanol, resulting in an ion of m/z 163. Loss of methanol accompanies a rearrangement from a 6-membered ring to a 5-membered ring.

A second, independent, fragmentation pathway also exists in which protonated ferulic acid undergoes loss of methanol to form an ion of m/z 163. Since direct protonation on the methoxy group is quite unfavourable (Figure 6.2), it is likely that proton transfer takes place. This presumably involves transfer of the phenolic proton to the adjacent methoxy group. Proton transfer directly from the $COOH_2^+$ group of the side chain by forming a "scorpion-

like" tail was also considered and successfully optimized ($\Delta G_{rel}°$ = 48.5 kJ/mol compared to Fer1b for m/z 195); however, it was found that the tail would not facilitate such a proton transfer.

Following proton transfer, a concerted rearrangement of the phenyl ring leads to formation of a five-membered ring, accompanying the loss of methanol. All attempts to find a six-membered ring structure of m/z 163 led spontaneously to collapse to the five-membered ring structure. The proposed structure and bond lengths of the 5-membered ring species are shown in Table 6.7 below. The bond lengths shown indicate that the resonance hybrid of m/z 163 is best represented by an acylium-type structure.

Table 6.7: The proposed structure for ion m/z 163 is in resonance between a ketene and acylium type species, and contains a five-membered ring. Significant atoms are labeled with numbers and bond lengths are shown in Angstroms (Å).

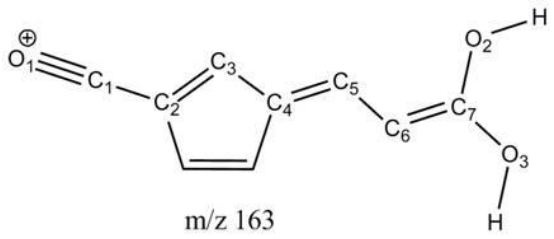

m/z 163

Atoms	Bond Length
O1 – C1	1.14
C1 – C2	1.35
C2 – C3	1.42
C3 – C4	1.41
C4 – C5	1.41
C5 – C6	1.39
C6 – C7	1.39
C7 – O2	1.31
C7 – O3	1.32

6.6 Conclusions

In summary, IRMPD spectroscopy experiments have shown that protonated ferulic acid produces three stable fragment ions of m/z 177, 149, and 163. The experimental IRMPD spectrum of this extensively conjugated species is matched exceptionally well by the anharmonic spectrum calculated at the B3LYP/6-311+G(d,p) level of theory. Protonated ferulic acid has been observed to undergo two unique fragmentation mechanisms during IRMPD experiments. In both fragmentation pathways, ferulic acid is initially protonated on the carbonyl oxygen. Scheme 1 shows that following IRMPD, proton transfer from the carbonyl to hydroxyl oxygen results in the loss of water, yielding an ion of m/z 177. Further isolation of the ion of m/z 177, followed by IRMPD, results in the loss of carbon monoxide to form an allene-like ion of m/z 149. In scheme 2, protonated ferulic acid undergoes proton transfer from the phenolic OH to the adjacent methoxy group, resulting in the loss of methanol and rearrangement to a five-membered ring. This work has again demonstrated that IRMPD spectroscopy, coupled with electronic structure calculations, can be a powerful technique for determining the mechanism of dissociation and the structure of ions in the gas phase.

Appendix A

The Complete Set of Calculated Low Energy Isomers (Within 15 kJ/mol of the Lowest Energy Isomer) for Uracil and 5-Fluorouracil

All geometry optimization and frequency calculations in Appendix A were performed at the MP2(full)/aug-cc-pVTZ level of theory.

The calculated isomers of neutral uracil.

Relative Gibbs free energies (298 K) are shown in kJ/mol.

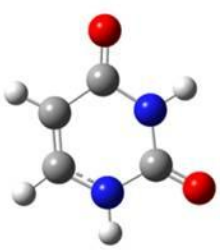

Neutral 01
0.0

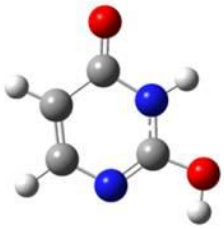

Neutral 02
41.7

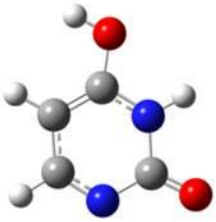

Neutral 03
83.3

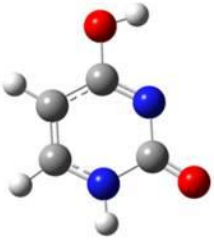

Neutral 04
45.4

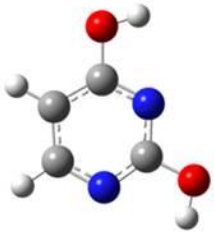

Neutral 05
41.4

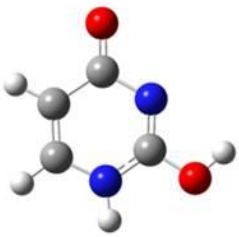

Neutral 06
72.4

The relevant calculated isomers of deprotonated uracil.

Relative Gibbs free energies (298 K) are shown in kJ/mol.

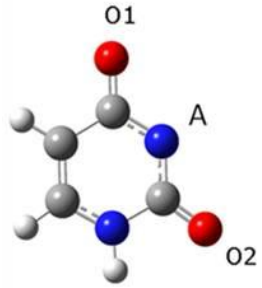

U-01-H

49.4

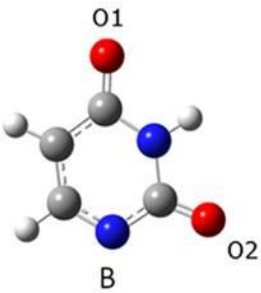

U-01-H2

0.0

The calculated lowest energy isomers for deprotonated uracil clustered with water.

Relative Gibbs free energies (298 K) are shown in kJ/mol.

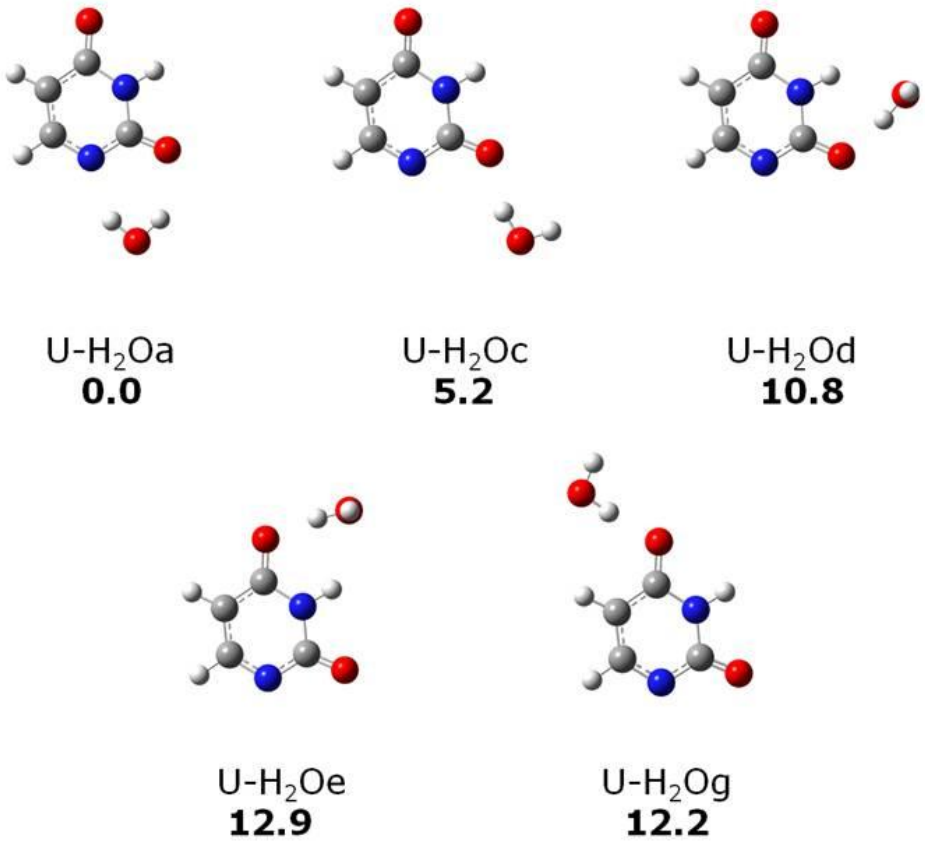

The calculated lowest energy isomers for deprotonated uracil clustered with methanol.

Relative Gibbs free energies (298 K) are shown in kJ/mol.

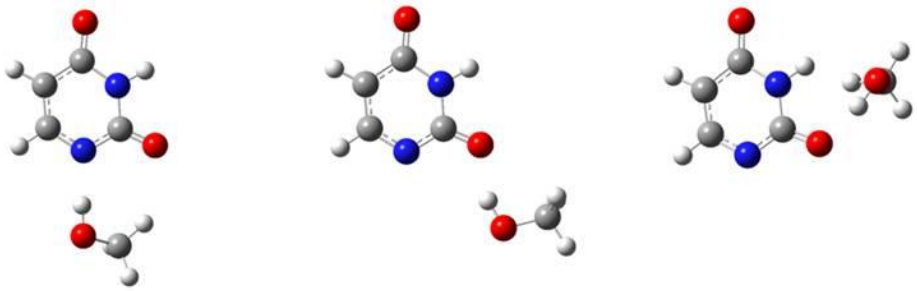

U-MeOHa
0.0

U-MeOHc
6.6

U-MeOHd
8.9

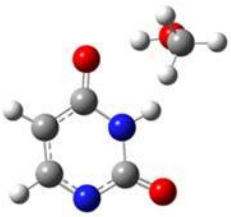

U-MeOHf
11.6

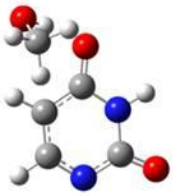

U-MeOHg
9.5

The calculated lowest energy isomers for deprotonated uracil clustered with ammonia.

Relative Gibbs free energies (298 K) are shown in kJ/mol.

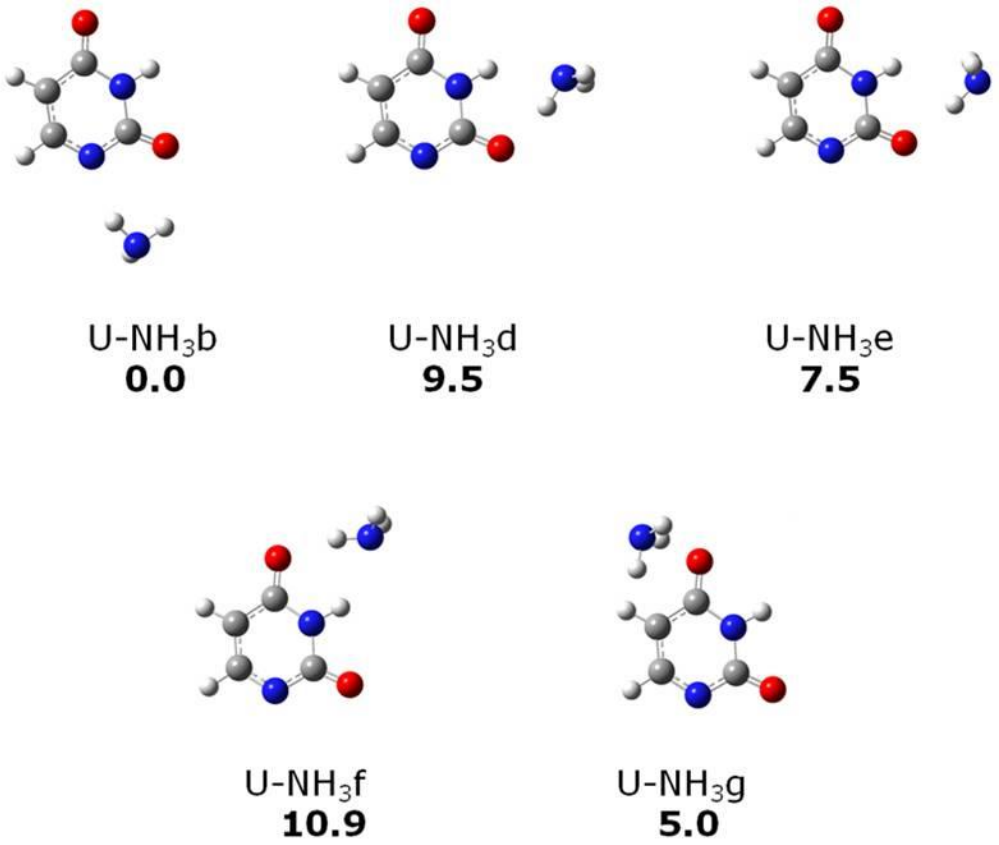

The calculated lowest energy isomers for deprotonated uracil clustered with methylamine.

Relative Gibbs free energies (298 K) are shown in kJ/mol.

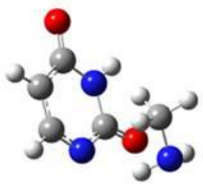

U-MeNH$_2$a
0.0

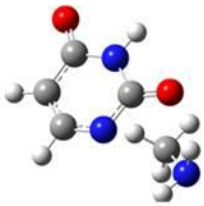

U-MeNH$_2$c
1.0

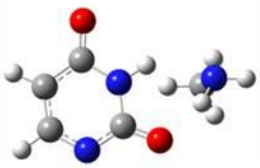

U-MeNH$_2$d
9.1

U-MeNH$_2$e
4.5

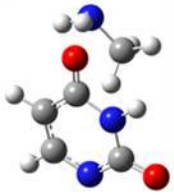

U-MeNH$_2$f
5.2

U-MeNH$_2$g
7.5

The calculated lowest energy isomers for deprotonated 5-fluorouracil clustered with water.

Relative Gibbs free energies (298 K) are shown in kJ/mol.

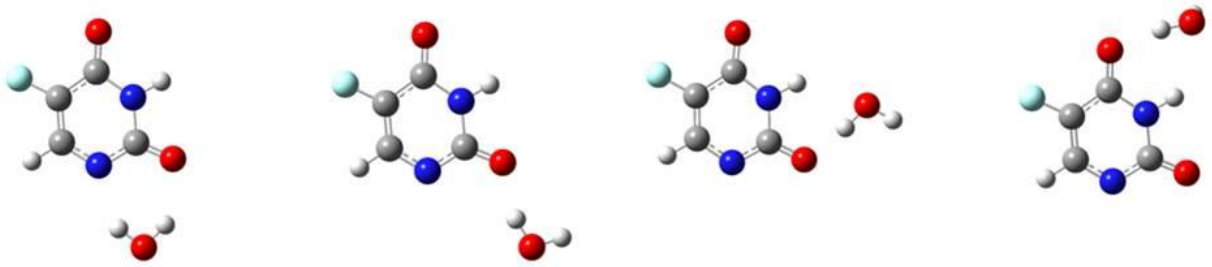

FU-H_2Oa **0.0**

FU-H_2Oc **3.4**

FU-H_2Od **11.7**

FU-H_2Of **14.3**

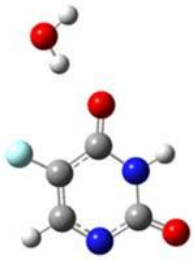

FU-H_2Og **9.4**

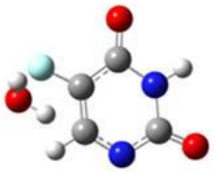

FU-H_2Oh **24.5**

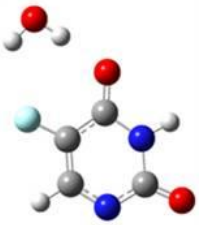

FU-H_2Oi **9.0**

The calculated lowest energy isomers for deprotonated 5-fluorouracil clustered with methanol.

Relative Gibbs free energies (298 K) are shown in kJ/mol.

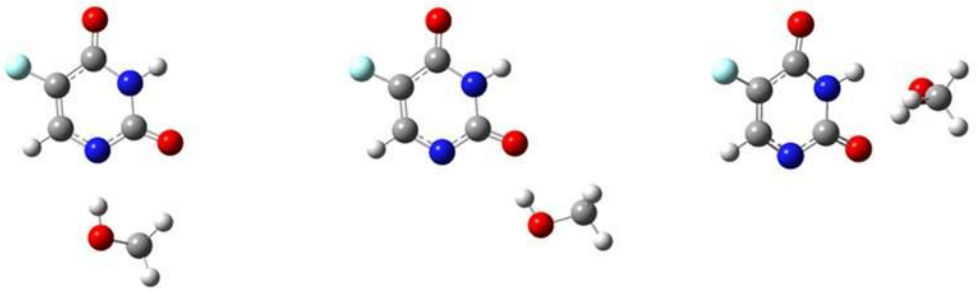

FU-MeOHa
0.0

FU-MeOHc
5.3

FU-MeOHd
6.8

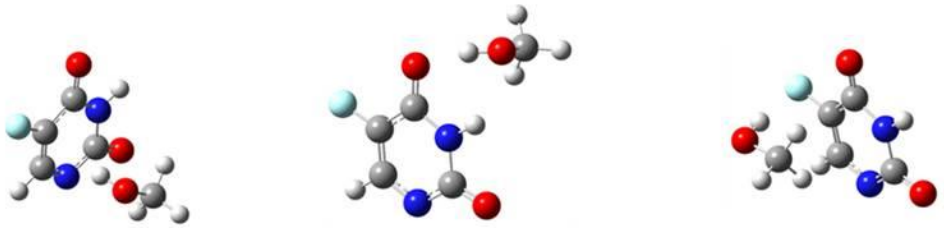

FU-MeOHe
22.6

FU-MeOHf
12.4

FU-MeOHi
22.4

The calculated lowest energy isomers for deprotonated 5-fluorouracil clustered with ammonia.

Relative Gibbs free energies (298 K) are shown in kJ/mol.

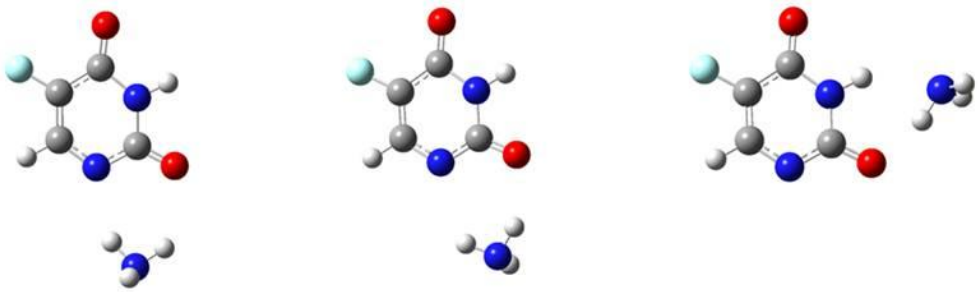

FU-NH_3a
2.6

FU-NH_3c
0.0

FU-NH_3d
11.7

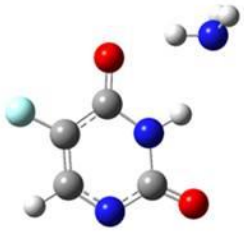

FU-NH_3f
14.6

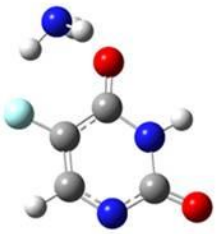

FU-NH_3g
8.7

The calculated lowest energy isomers for deprotonated 5-fluorouracil clustered with methylamine.

Relative Gibbs free energies (298 K) are shown in kJ/mol.

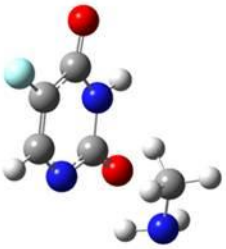

FU-MeNH$_2$a
0.0

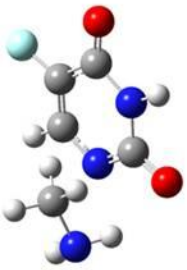

FU-MeNH$_2$c
1.6

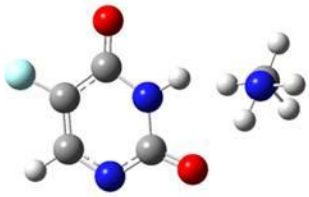

FU-MeNH$_2$d
8.8

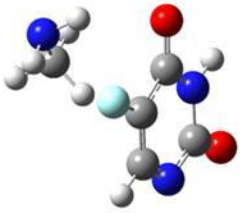

FU-MeNH$_2$f
5.0

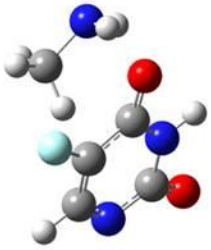

FU-MeNH$_2$g
5.8

Appendix B

Electronic Structure Calculations: A Sample Input File

%mem=12GB

%nproc=8

#mp2(full)/aug-cc-pvdz opt freq scale=0.969 nosymm

5-Fluorouracil cluster with water

-1 1

C	-1.19577200	-0.23790400	-0.86040500
N	-1.01001000	-1.59738000	-0.86716600
C	0.22815400	-2.04012700	-0.54894900
C	1.31865400	-1.25969500	-0.21126300
C	1.21926900	0.16533900	-0.17573800
N	-0.07054100	0.56816400	-0.52037700
H	0.37005600	-3.12805200	-0.55766500
O	-2.26718300	0.34670300	-1.12177400
O	2.11180700	1.00342200	0.12723900
F	2.52643300	-1.85299900	0.09406300
H	-0.24313500	1.57069300	-0.50084100
H	0.50263500	1.72838100	2.65485100
O	1.19177400	2.35774600	2.40866700
H	1.57255400	1.95954600	1.59691000

Bibliography

1. M. Meot-Ner, *Chemical Reviews*, 2005, **105**, 213-284.
2. R. Parthasarathi, V. Subramanian and N. Sathyamurthy, *The Journal of Physical Chemistry A*, 2006, **110**, 3349-3351.
3. M. Goswami and E. Arunan, *Physical Chemistry Chemical Physics*, 2009, **11**, 8974-8983.
4. L. Pauling, *The Chemical Bond: A brief Introduction to Modern Structural Chemistry*, Ithaca, New York, 1967.
5. J. Emsley, *Chemical Society Reviews*, 1980, **9**, 91-124.
6. K. A. Dill, *Biochemistry*, 1990, **29**, 7133-7155.
7. R. A. Marta, Doctor of Philosophy, University of Waterloo, 2009.
8. E. V. Anslyn and D. A. Dougherty, *Modern Physical Organic Chemistry*, University Science Books, United States of America, 2006.
9. *CRC Handbook of Chemistry and Physics*, 1971.
10. I. Dzidic and P. Kebarle, *The Journal of Physical Chemistry*, 1970, **74**, 1466-1474.
11. J. W. Larson and T. B. McMahon, *Journal of the American Chemical Society*, 1982, **104**, 6255-6261.
12. T. D. Fridgen, L. MacAleese, T. B. McMahon, J. Lemaire and P. Maitre, *Physical Chemistry Chemical Physics*, 2006, **8**, 955-966.
13. R. Wu and T. B. McMahon, *Journal of the American Chemical Society*, 2007, **129**, 4864-4865.
14. P. Ayotte, C. G. Bailey, G. H. Weddle and M. A. Johnson, *The Journal of Physical Chemistry A*, 1998, **102**, 3067-3071.
15. S. K. Silverman and T. R. Cech, *Biochemistry*, 1999, **38**, 8691-8702.
16. J. Šponer, J. Leszczynski and P. Hobza, *Biopolymers*, 2001, **61**, 3-31.
17. J. Brahms and C. Sadron, *Nature*, 1966, **212**, 1309-1312.
18. G. D. Rose and R. Wolfenden, *Annual Review of Biophysics and Biomolecular Structure*, 1993, **22**, 381-415.
19. W. Kabsch and C. Sander, *Biopolymers*, 1983, **22**, 2577-2637.
20. G. Newsome and G. Glish, *Journal of The American Society for Mass Spectrometry*, 2009, **20**, 1127-1131.
21. J. R. Eyler, *Mass Spectrometry Reviews*, 2009, **28**, 448-467.
22. T. Baer and W. L. Hase, *Unimolecular Reaction Dynamics. Theory and Experiments*, Oxford University Press, New York, NY, 1996.
23. J. S. Brodbelt and J. J. Wilson, *Mass Spectrometry Reviews*, 2009, **28**, 390-424.
24. C. S. Parmenter, *The Journal of Physical Chemistry*, 1982, **86**, 1735-1750.
25. J. Oomens, B. G. Sartakov, G. Meijer and G. von Helden, *International Journal of Mass Spectrometry*, 2006, **254**, 1-19.
26. M. A. Duncan, *International Journal of Mass Spectrometry*, 2000, **200**, 545-569.
27. D. M. Peiris, M. A. Cheeseman, R. Ramanathan and J. R. Eyler, *The Journal of Physical Chemistry*, 1993, **97**, 7839-7843.
28. R. Wu and T. B. McMahon, *Journal of the American Chemical Society*, 2007, **129**, 11312-11313.
29. K. Rajabi and T. D. Fridgen, *The Journal of Physical Chemistry A*, 2007, **112**, 23-30.
30. J. J. Valle, J. R. Eyler, J. Oomens, D. T. Moore, A. F. G. van der Meer, G. von Helden, G. Meijer, C. L. Hendrickson, A. G. Marshall and G. T. Blakney, *Review of Scientific Instruments*, 2005, **76**, 023103-023107.

31. N. C. Polfer, J. J. Valle, D. T. Moore, J. Oomens, J. R. Eyler and B. Bendiak, *Analytical Chemistry*, 2005, **78**, 670-679.
32. K. R. Asmis, G. Santambrogio, J. Zhou, E. Garand, J. Headrick, D. Goebbert, M. A. Johnson and D. M. Neumark, *The Journal of Chemical Physics*, 2007, **126**, 191105-191105.
33. D. Krajnovich, F. Huisken, Z. Zhang, Y. R. Shen and Y. T. Lee, *The Journal of Chemical Physics*, 1982, **77**, 5977-5989.
34. E. Würzberg, L. J. Kovalenko and P. L. Houston, *Chemical Physics*, 1978, **35**, 317-329.
35. J. L. Stephenson, M. M. Booth, J. A. Shalosky, J. R. Eyler and R. A. Yost, *Journal of The American Society for Mass Spectrometry*, 1994, **5**, 886-893.
36. D. S. Bomse, D. W. Berman and J. L. Beauchamp, *Journal of the American Chemical Society*, 1981, **103**, 3967-3971.
37. D. W. Noid and J. R. Stine, *Chemical Physics Letters*, 1979, **65**, 153-157.
38. R. A. Marta, R. Wu, K. R. Eldridge, J. K. Martens and T. B. McMahon, *Physical Chemistry Chemical Physics*, 2010, **12**, 3431-3442.
39. M. Okumura, L. I. Yeh and Y. T. Lee, *The Journal of Chemical Physics*, 1985, **83**, 3705-3706.
40. S. K. Shin and J. L. Beauchamp, *Journal of the American Chemical Society*, 1990, **112**, 2057-2066.
41. M. R. Zakin, R. O. Brickman, D. M. Cox, K. C. Reichmann, D. J. Trevor and A. Kaldor, *The Journal of Chemical Physics*, 1986, **85**, 1198-1199.
42. J. Oomens, N. Polfer, D. T. Moore, L. van der Meer, A. G. Marshall, J. R. Eyler, G. Meijer and G. von Helden, *Physical Chemistry Chemical Physics*, 2005, **7**, 1345-1348.
43. N. C. Polfer, J. Oomens and R. C. Dunbar, *Physical Chemistry Chemical Physics*, 2006, **8**, 2744-2751.
44. R. Wu and T. B. McMahon, *Mass Spectrometry Reviews*, 2009, **28**, 546-585.
45. D. Scuderi, C. F. Correia, O. P. Balaj, G. Ohanessian, J. Lemaire and P. Maitre, *ChemPhysChem*, 2009, **10**, 1630-1641.
46. R. Wu and T. B. McMahon, *The Journal of Physical Chemistry B*, 2009, **113**, 8767-8775.
47. R. H. Wu and T. B. McMahon, *ChemPhysChem*, 2008, **9**, 2826-2835.
48. S. H. Yoon, J. Chamot-Rooke, B. R. Perkins, A. E. Hilderbrand, J. C. Poutsma and V. H. Wysocki, *J. Am. Chem. Soc.*, 2008, **130**, 17644-17645.
49. M. S. Wilm and M. Mann, *International Journal of Mass Spectrometry and Ion Processes*, 1994, **136**, 167-180.
50. M. Yamashita and J. B. Fenn, *The Journal of Physical Chemistry*, 1984, **88**, 4451-4459.
51. J. B. Fenn, M. Mann, C. K. Meng, S. F. Wong and C. M. Whitehouse, *Mass Spectrometry Reviews*, 1990, **9**, 37-70.
52. N. B. Cech and C. G. Enke, *Mass Spectrometry Reviews*, 2001, **20**, 362-387.
53. J. V. Iribarne and B. A. Thomson, *The Journal of Chemical Physics*, 1976, **64**, 2287-2294.
54. G. J. Van Berkel, S. A. McLuckey and G. L. Glish, *Analytical Chemistry*, 1991, **63**, 1098-1109.
55. R. E. March, *Journal of Mass Spectrometry*, 1997, **32**, 351-369.
56. J. N. Louris, R. G. Cooks, J. E. P. Syka, P. E. Kelley, G. C. Stafford and J. F. J. Todd, *Analytical Chemistry*, 1987, **59**, 1677-1685.
57. R. E. Kaiser Jr, R. Graham Cooks, G. C. Stafford Jr, J. E. P. Syka and P. H. Hemberger, *International Journal of Mass Spectrometry and Ion Processes*, 1991, **106**, 79-115.
58. S. A. McLuckey, G. L. Glish and P. E. Kelley, *Analytical Chemistry*, 1987, **59**, 1670-1674.
59. D. Oepts, A. F. G. van der Meer and P. W. van Amersfoort, *Infrared Physics & Technology*, 1995, **36**, 297-308.

60. F. Glotin and A. Gayral, What is a Free-Electron laser?, http://clio.lcp.u-psud.fr/clio_eng/FEL.html, Accessed March 02, 2011.
61. P. Sprangle and R. A. Smith, *Physical Review A*, 1980, **21**, 293.
62. A. Renieri, *Endeavour*, 1984, **8**, 35-43.
63. D. A. G. Deacon, L. R. Elias, J. M. J. Madey, G. J. Ramian, H. A. Schwettman and T. I. Smith, *Physical Review Letters*, 1977, **38**, 892.
64. A. L. Heaton, V. N. Bowman, J. Oomens, J. D. Steill and P. B. Armentrout, *The Journal of Physical Chemistry A*, 2009, **113**, 5519-5530.
65. J.-Y. Salpin, S. Guillaumont, J. Tortajada, L. MacAleese, J. Lemaire and P. Maitre, *ChemPhysChem*, 2007, **8**, 2235-2244.
66. G. W. T. M. J. Frisch, H. B. Schlegel, G. E. Scuseria, M. A. Robb, J. R. Cheeseman, J. A. Montgomery, Jr., T. Vreven, K. N. Kudin, J. C. Burant, J. M. Millam, S. S. Iyengar, J. Tomasi, V. Barone, B. Mennucci, M. Cossi, G. Scalmani, N. Rega, G. A. Petersson, H. Nakatsuji, M. Hada, M. Ehara, K. Toyota, R. Fukuda, J. Hasegawa, M. Ishida, T. Nakajima, Y. Honda, O. Kitao, H. Nakai, M. Klene, X. Li, J. E. Knox, H. P. Hratchian, J. B. Cross, V. Bakken, C. Adamo, J. Jaramillo, R. Gomperts, R. E. Stratmann, O. Yazyev, A. J. Austin, R. Cammi, C. Pomelli, J. W. Ochterski, P. Y. Ayala, K. Morokuma, G. A. Voth, P. Salvador, J. J. Dannenberg, V. G. Zakrzewski, S. Dapprich, A. D. Daniels, M. C. Strain, O. Farkas, D. K. Malick, A. D. Rabuck, K. Raghavachari, J. B. Foresman, J. V. Ortiz, Q. Cui, A. G. Baboul, S. Clifford, J. Cioslowski, B. B. Stefanov, G. Liu, A. Liashenko, P. Piskorz, I. Komaromi, R. L. Martin, D. J. Fox, T. Keith, M. A. Al-Laham, C. Y. Peng, A. Nanayakkara, M. Challacombe, P. M. W. Gill, B. Johnson, W. Chen, M. W. Wong, C. Gonzalez, and J. A. Pople., Wallingford, CT, 2004.
67. G. W. T. M. J. Frisch, H. B. Schlegel, G. E. Scuseria, M. A. Robb, J. R. Cheeseman, G. Scalmani, V. Barone, B. Mennucci, G. A. Petersson, H. Nakatsuji, M. Caricato, X. Li, H. P. Hratchian, A. F. Izmaylov, J. Bloino, G. Zheng, J. L. Sonnenberg, M. Hada, M. Ehara, K. Toyota, R. Fukuda, J. Hasegawa, M. Ishida, T. Nakajima, Y. Honda, O. Kitao, H. Nakai, T. Vreven, J. A. Montgomery, Jr., J. E. Peralta, F. Ogliaro, M. Bearpark, J. J. Heyd, E. Brothers, K. N. Kudin, V. N. Staroverov, R. Kobayashi, J. Normand, K. Raghavachari, A. Rendell, J. C. Burant, S. S. Iyengar, J. Tomasi, M. Cossi, N. Rega, J. M. Millam, M. Klene, J. E. Knox, J. B. Cross, V. Bakken, C. Adamo, J. Jaramillo, R. Gomperts, R. E. Stratmann, O. Yazyev, A. J. Austin, R. Cammi, C. Pomelli, J. W. Ochterski, R. L. Martin, K. Morokuma, V. G. Zakrzewski, G. A. Voth, P. Salvador, J. J. Dannenberg, S. Dapprich, A. D. Daniels, Ö. Farkas, J. B. Foresman, J. V. Ortiz, J. Cioslowski, and D. J. Fox., Gaussian, Inc., Wallingford, CT, 2009.
68. T. K. a. J. M. Roy Dennington, Semichem Inc., Shawnee Mission, KS, 2009.
69. M. Mueller, *Fundamentals of Quantum Chemistry. Molecualr Spectroscopy and Modern Electronic Structure Calculations*, Kluwer Academic / Plenum Publishers, New York, NY, 2001.
70. E. Lewars, *Computational Chemistry. Introduction to the Theory and Applications of Molecular and Quantum Mechanics*, Kluwer Academic Publishers, Norwell, MA, 2003.
71. M. P. Andersson and P. Uvdal, *The Journal of Physical Chemistry A*, 2005, **109**, 2937-2941.
72. P. Sinha, S. E. Boesch, C. Gu, R. A. Wheeler and A. K. Wilson, *The Journal of Physical Chemistry A*, 2004, **108**, 9213-9217.
73. A. P. Scott and L. Radom, *The Journal of Physical Chemistry*, 1996, **100**, 16502-16513.
74. J. Simons, *An introduction to theoretical chemistry*, Press syndicate of hte university of Cambridge, Cambridge, UK, 2003.

75. J. B. Foresman and E. Frisch, *Exploring Chemistry with Electronic Structure Methods*, Gaussian, Inc, Pittsburgh, PA, 1995.
76. oslash, C. ller and M. S. Plesset, *Physical Review*, 1934, **46**, 618.
77. A. D. Becke, *The Journal of Chemical Physics*, 1993, **98**, 1372-1377.
78. J. P. Perdew, M. Ernzerhof and K. Burke, *The Journal of Chemical Physics*, 1996, **105**, 9982-9985.
79. M. Orio, D. Pantazis and F. Neese, *Photosynthesis Research*, 2009, **102**, 443-453.
80. S. Kossmann, B. Kirchner and F. Neese, *Molecular Physics: An International Journal at the Interface Between Chemistry and Physics*, 2007, **105**, 2049 - 2071.
81. J. C. Cramer, *Essentials of Computational Chemistry: Theories and Models.* , John Wiley & Sons Ltd., West Sussex, England, 2008.
82. S. Grimme, *The Journal of Chemical Physics*, 2006, **124**, 034108-034116.
83. R. N. Allen, P. Lipkowski, M. K. Shukla and J. Leszczynski, *Spectrochimica Acta Part A: Molecular and Biomolecular Spectroscopy*, 2007, **68**, 639-645.
84. H. Arslan and O. Algul, *Int. J. Mol. Sci.*, 2007, **8**, 760-776.
85. C. L. Bailey, S. Mukhopadhyay, A. Wander and N. M. Harrison, *J. Phys. Conf. Ser.*, 2009, **100**.
86. A. Sierraalta, G. Martorell, E. Ehrmann and R. Añez, *International Journal of Quantum Chemistry*, 2008, **108**, 1036-1043.
87. E. Szostak, K. Druzbicki and E. Mikuli, *Journal of Molecular Structure*, 2010, **970**, 139-146.
88. D. Zhao, J. Langer, J. Oomens and O. Dopfer, *The Journal of Chemical Physics*, 2009, **131**, 184307-184312.
89. J. T. H. Dunning, *The Journal of Chemical Physics*, 1989, **90**, 1007-1023.
90. D. Talbi and Y. Ellinger, *Chemical Physics Letters*, 1996, **263**, 385-392.
91. D. Talbi, Y. Ellinger and E. Herbst, *Astron Astrophys*, 1996, **314**, 688-692.
92. T. Schwabe and S. Grimme, *Physical Chemistry Chemical Physics*, 2007, **9**, 3397-3406.
93. M. O. Sinnokrot, E. F. Valeev and C. D. Sherrill, *Journal of the American Chemical Society*, 2002, **124**, 10887-10893.
94. R. Wu and T. B. McMahon, *J. Mass Spectrom.*, 2008, **43**, 1641-1648.
95. R. L. Myers, in *The 100 most important chemical compounds: a reference guide*, Greenwood Publishing Group, 2007, pp. 92-93.
96. W. B. Parker and Y. C. Cheng, *Pharmacology & Therapeutics*, 1990, **48**, 381-395.
97. R. B. Diasio and B. E. Harris, *Clinical Pharmacokinetics*, 1989, **16**, 215-237.
98. D. B. Longley, D. P. Harkin and P. G. Johnston, *Nat Rev Cancer*, 2003, **3**, 330-338.
99. S. S. Cohen, J. G. Flaks, H. D. Barner, M. R. Loeb and J. Lichtenstein, *Proceedings of the National Academy of Sciences of the United States of America*, 1958, **44**, 1004-1012.
100. C. G. Atkins, L. Banu, M. Rowsell, V. Blagojevic, D. K. Bohme and T. D. Fridgen, *The Journal of Physical Chemistry B*, 2009, **113**, 14457-14464.
101. M. Kurinovich and J. Lee, *Journal of The American Society for Mass Spectrometry*, 2002, **13**, 985-995.
102. T. M. Miller, S. T. Arnold, A. A. Viggiano and A. E. Stevens Miller, *The Journal of Physical Chemistry A*, 2004, **108**, 3439-3446.
103. A. R. Waldorf and A. Polak, *Antimicrob. Agents Chemother.*, 1983, **23**, 79-85.
104. R. B. Diasio, J. E. Bennett and C. E. Myers, *Biochemical Pharmacology*, 1978, **27**, 703-707.
105. M. A. Ghannoum and L. B. Rice, *Clin. Microbiol. Rev.*, 1999, **12**, 501-517.
106. J. Murgich, H. J. Franco and G. San-Blas, *J. Phys. Chem. A*, 2006, **110**, 10106-10115.
107. J. Desjardins, D. L. Emerson, D. B. Colagiovanni, E. Abbott, E. N. Brown and D. W. Drolet, *J. Pharmacol. Exp. Ther.*, 2004, **309**, 894-902.

108. P. D. Boucher, N. M. Im, S. O. Freytag and D. S. Shewach, *Cancer Res.*, 2006, **66**, 3230-3237.
109. J. P. Merrick, D. Moran and L. Radom, *The Journal of Physical Chemistry A*, 2007, **111**, 11683-11700.
110. H. A. Galue, O. Pirali and J. Oomens, *Astron. Astrophys.*, 2010, **517**.
111. E. P. L. Hunter and S. G. Lias, *J. Phys. Chem. Ref. Data*, 1998, **27**, 413-656.
112. G. M. Chaban, J. O. Jung and R. B. Gerber, *The Journal of Physical Chemistry A*, 2000, **104**, 10035-10044.
113. G. M. Chaban, J. O. Jung and R. B. Gerber, *The Journal of Physical Chemistry A*, 2000, **104**, 2772-2779.
114. U. Buck, J.-G. Siebers and R. J. Wheatley, *The Journal of Chemical Physics*, 1998, **108**, 20-32.
115. A. A. Adesokan and R. B. Gerber, *The Journal of Physical Chemistry A*, 2008, **113**, 1905-1912.
116. P. G. Wenthold and R. R. Squires, *The Journal of Physical Chemistry*, 1995, **99**, 2002-2005.
117. S. Mathew and T. E. Abraham, *Critical Reviews in Biotechnology*, 2004, **24**, 59-83.
118. K. Iiyama, T. B. T. Lam and B. A. Stone, *Plant Physiol.*, 1994, **104**, 315-320.
119. M. Casolaro, C. Anselmi and G. Picciocchi, *Thermochimica Acta*, 2005, **425**, 143-147.
120. P. J. Harris and R. D. Hartley, *Nature*, 1976, **259**, 508-510.
121. H. Kikuzaki, M. Hisamoto, K. Hirose, K. Akiyama and H. Taniguchi, *Journal of Agricultural and Food Chemistry*, 2002, **50**, 2161-2168.
122. E. Graf, *Free Radical Biology and Medicine*, 1992, **13**, 435-448.
123. D. K. Maurya and T. P. A. Devasagayam, *Food Chem. Toxicol.*, 2010, **48**, 3369-3373.
124. M. Srinivasan, A. R. Sudheer and V. P. Menon, *Journal of Clinical Biochemistry and Nutrition*, 2007, **40**, 92-100.
125. *USA Pat.*, 1993.
126. J. Pokorný, *Trends in Food Science & Technology*, 1991, **2**, 223-227.
127. M. Gardner, N. Li, A. Ellington and J. Brodbelt, *Journal of The American Society for Mass Spectrometry*, 2010, **21**, 580-591.
128. P. I. Surjasasmita and B. S. Freiser, *Journal of The American Society for Mass Spectrometry*, 1993, **4**, 135-144.
129. C. Parr and J. S. Brodbelt, *Journal of Mass Spectrometry*, 2010, **45**, 1098-1103.